Magnetic Resonance Imaging of TMJ

10

Kaan Orhan and Seçil Aksoy

10.1 Principle of Magnetic Resonance Imaging (MRI)

Magnetic resonance imaging (MRI) is a noninvasive imaging modality which is based on the nuclear magnetic resonance (NMR). Isıdor Isaac Rabi discovered and observed the NMR process. Rabi is the first to use the "nuclear magnetic resonance (NMR)" term by publishing an article entitled "A New Method of Measuring Nuclear Magnetic Moment." In 1944 Rabi was awarded with the Nobel Prize in Physics. Paul Lauterbur and Peter Mansfield used NMR to produce images of the body [1].

In MRI, short radio-frequency (RF) pulse is used to produce the excellent soft tissue images instead of the other imaging techniques using ionizing radiation. MRI machine has three basic components. Magnet is the biggest and most important component of the MRI machine, generating strong magnetic field to realign the body's atoms. Strength of the magnetic field is defined by the units of Tesla (T). There are five types of magnets used in MRI system including permanent magnets, electromagnets (solenoid), resistive magnets, superconducting magnets, and hybrid magnets [2]. In 95% of the MRI machine, superconducting magnets are used to generate the strong and highly homogeneous magnetic field. Superconducting magnet consists of a main coil wound up with niobium-titanium (NbTi) wires that have no resistance to the flow of an electrical current and creates a magnetic field of up to 18 T. The gradient system which is used for slice selection and spatial encoding of the signal produce an additional magnetic field in the direction of the x, y, and z axes. Radio-frequency systems compromise RF transmitter and a highly sensitive receiver that produce the RF waves, excite the nuclei, select the slices, apply the gradients, and are used in signal

K. Orhan (✉)
Department of Dentomaxillofacial Radiology, Ankara University, Faculty of Dentistry, Ankara, Turkey

S. Aksoy
Department of Dentomaxillofacial Radiology, Near East University, Faculty of Dentistry, Mersin, Turkey

acquisition [3]. Externally applied magnetic field effects the specific magnetic nuclei, such as hydrogen (^{1}H), carbon (^{13}C), fluorine (^{19}F), sodium (^{23}Na), oxygen (^{17}O), nitrogen (^{15}N), and phosphor (^{31}P). These atoms are called NMR active atoms [2].

10.1.1 Protons

All the materials in the world are made from atoms. Atoms are composed of particles called protons, neutrons, and electrons. Atomic nucleus consists of the protons and neutrons are called nucleons together. Total number of the protons and neutrons give the atomic mass number. Electrons move around the nucleus in orbitals. The protons and neutrons are attracted to each other by a nuclear force that holds them together in the nucleus at a certain distance [1]. Proton and neutrons revolve around themselves; therefore nuclear magnetism consists of the movement of these particles, and this magnetism is used to produce MR images. The number of neutrons relative to the protons determines the stability of the nucleus. Proton and neutrons both act as a small magnet with the south and north poles, and in equilibrium situations, net magnetic moment of the atom is zero. Nuclear magnetism is only seen in atoms with odd atomic mass number [2, 4–7].

The magnetism generated by nucleon particles is very weak, so to get an image, billions of atoms are needed. For this reason, hydrogen isotope, which has only a proton and no neutron in its nucleus, is the most suitable atom for MRI because it is the most abundant atom in human body, especially in water and fat. The high concentration of hydrogen nuclei in the human body, coupled with its high "relative MR sensitivity," makes the nucleus most suitable for high-resolution MRI [2, 8].

The magnetic moment of the particles in the nucleus spinning around itself is parallel to the rotation axis. This magnetic moment, created by the protons, is directly related to the rotation of the protons around themselves, and this spinning motion is called the spin or angular momentum. Magnetic moment is defined by the vector system which shows the power and direction of the magnetic field. Hydrogen atom which behaves like a small magnet and planet earth has a south and north pole and a magnetic vector (Fig. 10.1). The spin vectors of protons within the normal tissue are randomly oriented in all directions [7, 9, 10].
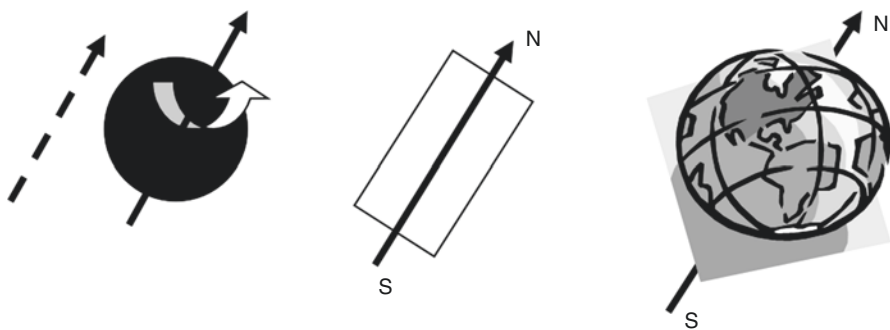

Fig. 10.1 Hydrogen atoms can be visualized as a small magnet or planet earth with a "north" and "south" pole

Once an external magnetic field (B_0) is applied, protons either align with (parallel/spin-up/low energy level) or against (anti parallel/spin-down/high energy level) it. However a slight excess of spins align parallel to the main magnetic field, causing net tissue magnetization. As the strength of the magnetic field increases, the number of parallel aligned atoms increases to [2–4, 7, 11].

10.1.2 Precession/Resonance

The magnetic vectors of protons do not align parallel or antiparallel exactly with the direction of the magnetic field (B_0). If an external magnetic field effects on a spinning protons and tries to change the orientation of the rotational axis, a second movement occurs, and protons begin to process at a rate known as the Larmor frequency around the lines of the applied magnetic field (Fig. 10.2); this process is called precession or oscillation [1–3, 7].

The frequency of the precession depends on the nature of the nucleus and on the strength of the external applied magnetic field. MRI scanners come in different field strength usually between 0.1 and 7 T with 1.5–3 T being the most common [7]. Larmor frequency (precession frequency or resonance frequency) is 63.86 MHz for the hydrogen atoms in a magnetic field of 1.5 T, and each magnetic nucleus has a special frequency in the same magnetic field [2, 5, 7]. Exposure of individual nuclei to RF pulse at the Larmor frequency causes nuclei in the lower energy state to reach into the higher energy state. Applications of the RF pulse cause the protons to change their magnetization alignment, and this newly formed magnetic vector is called transverse magnetization. Protons undergo a transition between the two energy states by the absorption of RF pulse, and after a while, they emitted the energy to return to their former position, which is called resonance [2, 3, 7].

Fig. 10.2 Precession. Each spinning hydrogen nucleus process around the direction of the external magnetic field, B_0, at the Larmor frequency

B_0 (Applied external magnetic field vector)

N

S
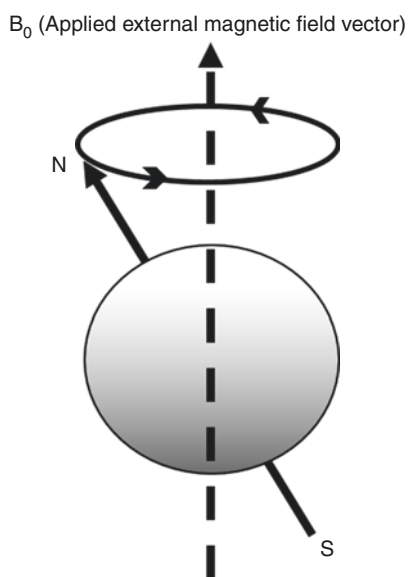
10.1.3 The Fundamentals of MRI

The transmission of the energy occurs in two ways within the tissue. These two independent processes reduce transverse magnetization and thus cause a return to the stable state present before excitation: spin-lattice interaction (longitudinal, thermal relaxation) and spin-spin interaction (transvers relaxation). These two processes cause T1 relaxation and T2 relaxation, respectively [3, 12]. The nuclei which precess around the direction of an applied magnetic field are out of phase initially. Application of the RF pulse causes the nuclei to precess in phase synchronously, and MR signal is formed, but it fades quickly, and nuclei become out of phase [6].

When a 90° RF pulse is applied to longitudinal magnetization, it tips down so that it creates transverse magnetization, an excited condition (Fig. 10.3).

RF pulse is usually applied in short pulses, each lasting microseconds, and when it is terminated, over a period of time, the nuclei return to its original longitudinal alignment (z axes), and energy is emitted from the tissue on relaxation [6, 11]. Absorption and vice versa emission of the energy induces an electric voltage or signal that can be detected by a receiver coil known as free induction decay (FID) [9, 11]. However, the MR signal quickly fades away due to the inhomogeneity in the magnetic field and microscopic local changes in the magnetic field (Fig. 10.4). The signal is lost in the milliseconds due to these reasons, and transverse relaxation which is caused by static magnetic field inhomogeneity and microscopic magnetic local differences is called T2* (T2 star) [9].

A 90° RF pulse application causes the net magnetization vector from the longitudinal plan into transverse plane which generates the detectable MR signal by a receiver coil positioned in this plane [2]. However if a uniform field of identical strength were generated throughout the body, RF pulse would excite all of the protons without a means of spatial localization, and signal would be detected from the whole body. To enable selected slice excitations, gradients should be used to produce deliberate variations in the main magnetic field. Thus, the Larmor frequencies of the protons outside the selected slice would change and would not be affected by
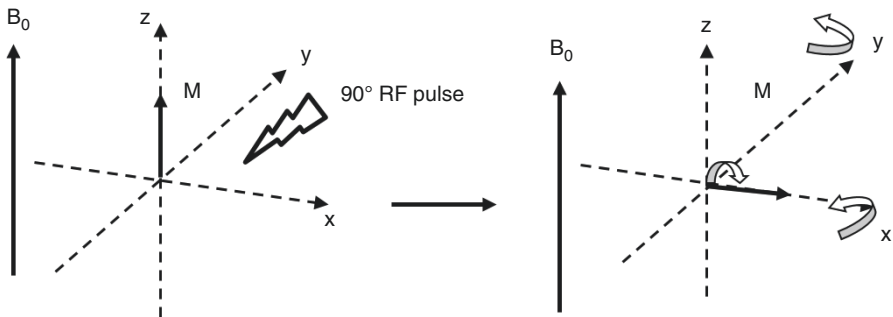

Fig. 10.3 In the presence of a magnetic field, net longitudinal magnetization occur in the z axis, and after a 90° RF pulse application, longitudinal magnetization tips down and rotate into transverse magnetization
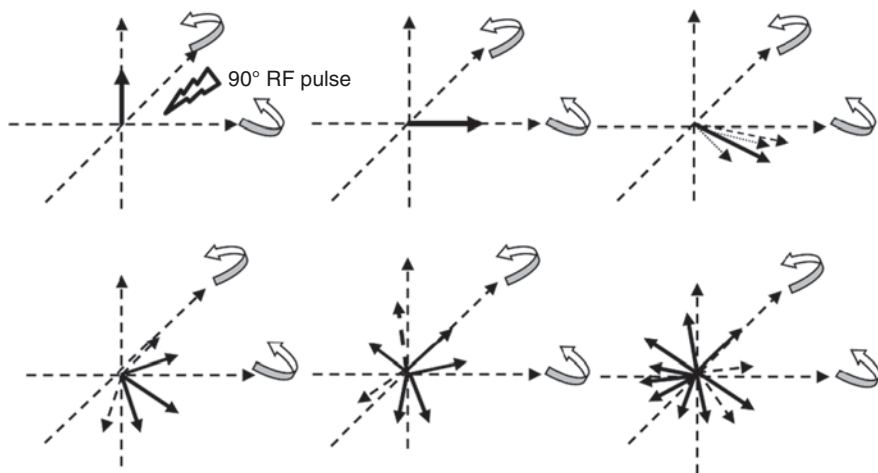
Fig. 10.4 Transverse magnetization is at maximum while the protons are in phase, due to the inter- and intramolecular interactions, protons begin to precess at different frequencies

the excitation pulse [3]. Gradient coils alter both the magnetic field magnitude and linear fashion so that a specific point along the axis of the gradient has a specific precessional frequency. This is known spatial encoding. Three sets of gradient coils are used in MR system one for each direction, and these are named according to the axis along which they act when they are switched on. Gradients accomplish the spatial localization in MRI, including slice selection, frequency encoding, and phase encoding. The location of the slice may be changed or moved along the slice selection gradient [2]. Slice thickness is determined by the amplitude of slice selection gradient and transmit bandwidth; shallow (weaker) gradient and broad transmit bandwidth generate thick slice, whereas steeper (strong) gradient and narrow transmit bandwidth generate thin slices [2, 3]. Frequency-encoding gradient that causes the precessional frequency of signal within the slice to be position along the axis of the gradient is changed in a linear fashion. Phase-encoding gradient is the spatial position of a signal along the short axis of the anatomy. The data are collected from all the gradients and stored into an array called k-space. K-space has two axes perpendicular to each other, while the horizontal axes represent the frequency information, vertical axes represent the phase information [2].

When the inhomogeneity of the magnet is reduced, the minimum there will only be transverse relaxation resulting from the microscopic local changes in the magnetic field that is called T2 or spin-echo relaxation. So perfectly homogeneous magnet is not possible; the influence of magnetic field inhomogeneity may be reduced by applying a 180° RF pulse. This method or sequence in which 180° RF pulses are used after 90° RF pulses is called the spin-echo (SE) sequence [3].

Determination of the amount of weighting depends on the acquisition parameters. Repetition time (TR) is the amount of the time from the application of an excitation pulse to the application of the next pulse and is therefore crucial for T1

contrast. T1 relaxation is the release of energy to the environment by which net magnetization vector recovers to its ground state in the direction of B_0 reaches thermodynamic equilibrium with its surroundings (the "lattice"). After the RF pulse has been applied, the signal will recover to 63% of its equilibrium value by this transfer of energy called T1 relaxation time [2, 6, 9, 11, 13]. Due to the different molecular structure in each tissue, it exhibits various T1 times. Application of shorter repetition times allows only partial recovery of tissue and the image contrast mainly affected by T1. The appearance of the tissue having a short T1 relaxation time such as fat on T1-weighted (T1W) image will appear as a bright because this tissue produces a stronger MR signal and has the highest level of magnetization at any particular time. On the other hand, a tissue with long T1 relaxation time such as cerebrospinal fluid produces weaker MR signals than tissue with short T1 and also appears dark because they do not regain their longitudinal magnetization on T1W images [2, 7, 13].

The time between the applications of the 90° RF pulse and MR signal sampling is called echo time (TE). The amount of the T2 relaxation is determined by TE. Short TE application results in the low T2 weighting, while long TE application results in the strong T2 weighting. Tissues with a long T2 relaxation time appear dark, whereas tissues with short T2 relaxation time such as cerebrospinal fluid appear bright on T2-weighted image [2, 7, 13].

10.1.4 Pixel/Voxel

Matrix of pixel or picture element is the smallest two-dimensional (2D) component of a digital image. Each pixel has 2D grid of row and columns determining the spatial resolution in-plane. This grid of pixels will hold signal intensity collected from the patient. A voxel is a rectangular cuboid volume element representing a value in the three-dimensional space, whose dimensions are set by the slice thickness, field of view (FOV), and matrix size by the scanning process [3, 14]. The voxel size represents the spatial resolution. The smaller the voxel, the greater the resolution.

10.1.5 Signal-to-Noise Ratio (SNR)

SNR is the quantitative value to the strength of the desired signal to its background reflections at a given point in time. The SNR in MRI depends on a slice thickness, receiver bandwidth, FOV, size of the (image) matrix, number of excitations (NEX), scan parameters (repetition time (TR), echo time (TE), flip angle), magnetic field strength, and selection of the transmit and receive coil (RF coil). SNR is proportional to the pixel size (FOV/matrix), slice thickness, number of excitations (NEX), and magnetic field strength, employing local coil, TR, and is inversely proportional to the receiver bandwidth, TE [3]. The higher the SNR in MR image, the more likely is the image quality. Noise is always present at the MRI, and even if the signal is

high, the quality of the view will be low if the noise is high. The use of surface coil system can trade for increased image detail by using smaller voxels and influence both the statistical and the spatial distribution of noise [15].

10.1.6 Contrast-to-Noise Ratio (CNR)

CNR is the ability to differentiate two adjacent structures of high signal from areas of low signal such as gray and white matter, scaled to image noise [16]. The CNR increases with the T2-weighted images, contrast agents, chemical pre-saturation technique, and magnetization transfer contrast [2].

10.2 Image Acquisition in MRI (Common Sequences in MRI for TMJ)

The names of various sequences used by the MR manufacturers are listed in Table 10.1.

10.2.1 T1, T2, and Proton Density-Weighted Spin-Echo Images

The most commonly used sequence is spin echo. Because imaging appearance may vary depending on the acquisition parameters, T1, T2, and proton density (PD)-weighted images are obtained by changing the TR and TE (Table 10.2) [2, 4, 17].

T1W images tend to have short TR (typically 300–700 ms) and TE (20 ms) and best demonstrate the anatomy. Fat has high signal intensity and appears bright on T1W images, whereas the lower signal for more water content such as edema, tumor, infarction, inflammation, infection, and CSF will be dark. A contrast agent usually shortened the value of the T1 and brightened the image. Also subacute hemorrhage, melanin, protein-rich fluid, and slowly flowing blood have high signal intensity on T1W images [7] (Fig. 10.5).

Unlike the T1W images, T2W images are produced by using long TR (2000 ms) and TE (typically ≥60 ms). Since fluid has a long T2 relaxation time, edema, tumor, infarction, inflammation, infection, CSF, and subacute hemorrhage appear bright, while contrast agent, calcification, fat, protein-rich fluid, and flow void appear dark on T2W images. T2W images are appropriate and most frequently used for visualizing the pathologic conditions [7] (Fig. 10.6).

Proton density (PD)-weighted image tends to have long TR (to diminish the T1 effect) and short TE (to diminish the T2 effect) [17]. PDW images display the amount of the protons per unit tissue. Fat exhibits relatively high signal intensity but not as bright as in T1W image. Fluid presents intermediate signal on PDW images [3]. Also PDW images provide better contrast between gray and white matter rather than T2W. PDW imaging is particularly helpful to differentiate the CSF and pathology which have both high signals on T2W images [18] (Fig. 10.7).

Table 10.1 The list of the common names for MRI sequences abbreviations used by different manufacturers

	Common names for MRI sequences abbreviations used by different manufacturers								
	Philips	GE	Hitachi	Siemens	Fonar	Toshiba	Elscint	Shimadzu	Picker
Spin echo	SE	SE, MEMP, VEMP	SE	SE	SE	SE	SE	SE	SE
Turbo spin echo/fast spin echo	TSE	FSE	FSE	TSE	FSE	FSE	FSE	RISE	FSE
Single shot technique	Single shot TSE	SSFSE	Single shot FSE	HASTE		FASE			EXPRESS
Gradient echo	FFE	GRE, GRASS	GE	GRE	Field echo	Field echo	SHORT	Field echo	FAST
Coherent gradient echo	FFE	GRASS, FGR, FMPGR	Rephased, SARGE, GFEC	FISP	Field echo	Field echo	E/F SHORT	SSFP	FAST
Incoherent gradient echo (RF spoiled)	T1 FFE	SPGR	GE/GFE	FLASH	Field echo	Field echo	SHORT	STAGE T1W	RF spoiled FAST
Incoherent gradient echo (gradient spoiled)	T2 FFE	MPGR	GRE	FLASH	Field echo	Field echo	SHORT	STAGE	T1-FAST NOSE
Steady-state free precession	T2 FFE	SSFP, DE FGR	Time reversed SARGE	PSIF	Field echo		F/E SHORT	STERF	CE FAST
Balanced sequences/true FISP	Balanced FFE	FIESTA	BASG	True FISP		True SSFP		STERF	
True FISP/dual excitation		FIESTA-C		CISS					
Multi-echo data image combination	M-FFE	MERGE	ADAGE	MEDIC					
Inversion recovery	IR, IR-TSE	IR, MPIR, FASTIR	IR	IR, TIR	IR	IR	IR	IR	IR
Short T1 inversion recovery	STIR	STIR	STIR	STIR	STIR	STIR	STIR	STIR	STIR
Long tau inversion recovery	FLAIR	FLAIR	Fast FLAIR	Turbo dark fluid					
True inversion recovery	Real IR	T1 FLAIR	T1 FLAIR	True IR					
	Philips	GE	Hitachi	Siemens	Fonar	Toshiba	Elscint	Shimadzu	Picker

Table 10.2 Relative TR and TE differences in basic spin-echo sequences

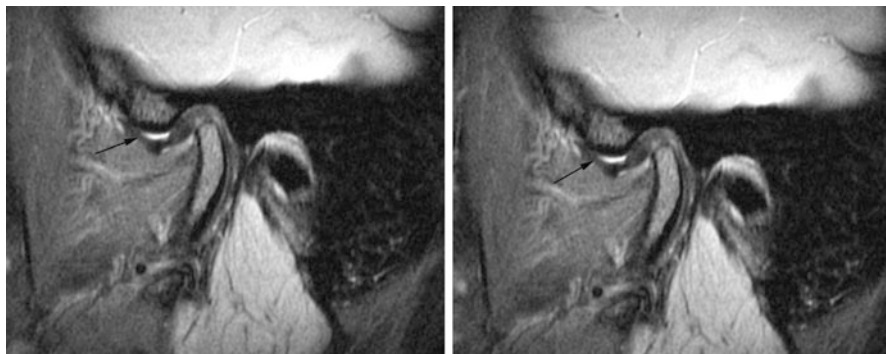|	TR	TE
T1 weighted	Short	Short
T2 weighted	Long	Long
Proton density weighted	Long	Short

Fig. 10.5 T1-W sagittal MR image showing anatomical structures of TMJ clearly with superior joint compartment effusion (arrows)
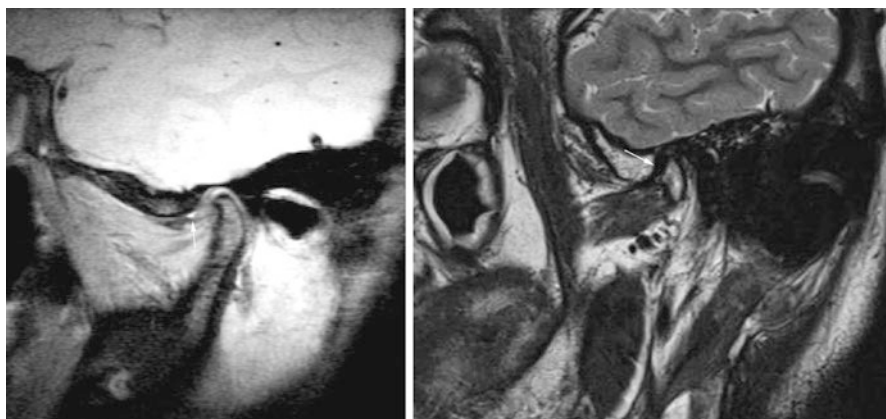

Fig. 10.6 MR image showing T1-W with effusion (white arrow) and T2-W sagittal images with degeneration of the condyle (black arrow)

10.2.2 Fast Spin Echo (FSE) and Turbo Spin-Echo Imaging (TSE)

Standard spin-echo sequences have relatively long acquisition times. Such an exemplary the acquisition time of a single T1W spin echo takes approximately 4 min; for T2W spin-echo image, this time increases 21 min with a 512 matrix size [17]. Conventional spin-echo sequences fill the k-space line by line until the entire space is filled per TR and scan time is very long. TR, number of excitations (NEX), and number of phase encodings affect the scan time and any changes in these parameter
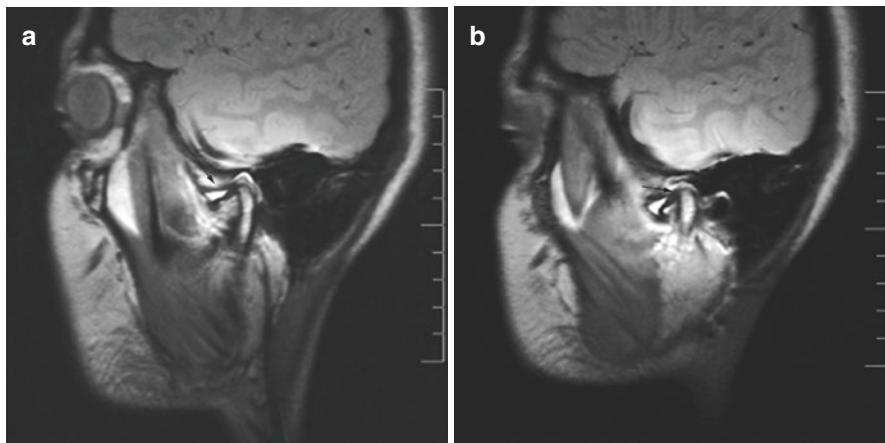
Fig. 10.7 (**a**) Proton-weighted sagittal MR images showing closed mouth and (**b**) open mouth position of a stuck disc (arrows)

image weighting, spatial resolution, and SNR in a negative way [2]. To decrease the acquisition time and reduce the motion artifact due to the long scan time, Hennig et al. developed the RARE (rapid acquisition with relaxation enhancement) sequence [19]. FSE sequence also called TSE depending on the manufacturers is characterized by multiple rapidly applied 180° rephrasing RF pulses after just one 90° excitation pulse and multiple echoes, to produce echo train. This number of the echoes is called echo train length (also known as the turbo factor). Instead of the one line in conventional spin-echo sequence, multiple lines are used to fill the k-space more rapidly in FSE sequences, and the scan time is decreased [2, 20]. Echo train length or turbo factor has an important role in image weighting. If the turbo factor is so high, scan time decrease, but image would be a mixture of weighting. To obtain a T1 and PDW fast spin-echo image, turbo factor has to be minimum, but in T2W image, larger turbo factor is needed [2] (Fig. 10.8).

10.2.3 Fat-Saturated TMJ Imaging

Since the majority of the body is composed of water and fat, these two parts constitute the major component of MR images. A relative difference in nuclear magnetic resonance frequency of the same water and fat's atomic nuclei depending on its molecular or molecular sites differences is known as chemical shift. If both water and lipid protons coexist in the same voxel, the signal from water and fat will be additive, and the out-of-phase transverse magnetization cancel each other out [3]. In clinical MR imaging, to prevent the signal loss, chemically selective RF pulses are applied to cause the signal from fat (or water) to be nulled (saturated), while the other signal is relatively unaffected before imaging [3, 5]. Fat suppression with chemically selective pulses is mainly used to suppress the signal coming from the
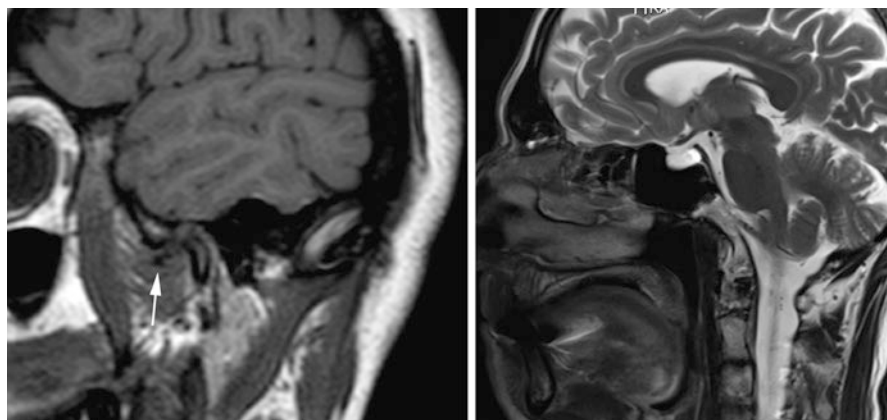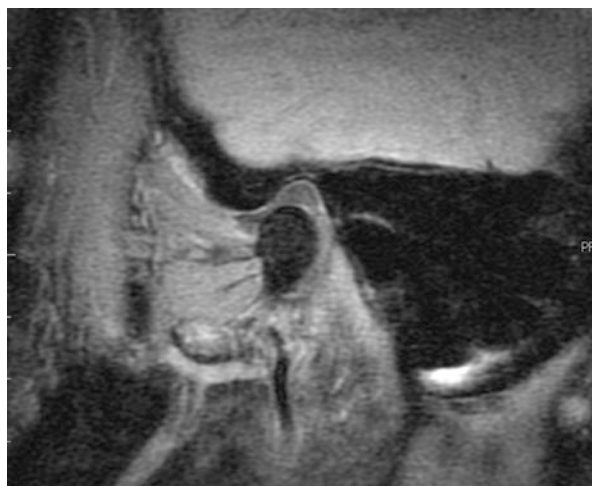
Fig. 10.9 T1- and T2-weighted STIR images. Note the disc displacement in the closed mouth position (arrow)

normal adipose tissue which causes the chemical shift artifact, to improve the visibility of the interested tissue, adrenal gland tumors, steatosis [21], fatty tumors (such as lipoma or liposarcoma), bone marrow edema, and extent of the pathologic lesion in the bone marrow [4].

As the fat saturation pulses are affected by the magnet inhomogeneity, highly uniform magnet is needed to obtain fat-saturated (FatSat) image. Inhomogeneity of the magnet results in partially saturated missing or incomplete fat [4]. A short frequency 90° fat sat pulse is applied; the fat protons magnetization deflected into the transverse plane before sequence imaging, and they produce no signal [20].

There are several techniques to achieve fat suppression including frequency-selective fat saturation (FS) and short-tau inversion recovery (STIR) (Fig. 10.9).

Dixon and spectral-attenuated inversionrecovery (SPAIR) techniques are the most commonly used two fat suppression methods [22]. Dixon technique is depending on the water/fat chemical shift differences. This technique is able to separate water and fat proton signals which are generated for in-phase and opposed-phase images, and then "fat-suppressed" water-only and "water-suppressed" fat-only images could be analytically calculated [22, 23] (Fig. 10.10).

10.2.4 Pseudo-Dynamic Imaging of TMJ

Pseudo-dynamic images is based on the static sequential step-by-step acquisitions which is obtained from the closed mouth to maximum open mouth position in various degree of the translation using bite block or mouth wedge [24, 25]. Pseudo-dynamic images can be played in cine loop to do a simulation of condylar movement [26]. Pseudo-dynamic image is not a real dynamic image; it is an artificial movement of the disc and condyle of the TMJ; physiological and pathological situations cannot directly visualize with this method [24, 25].
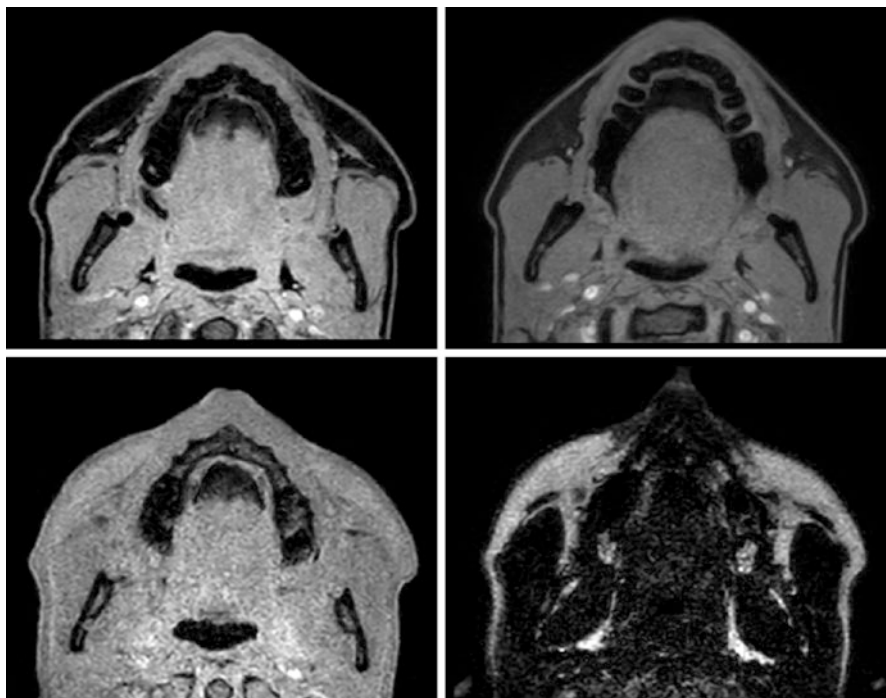

Fig. 10.10 Dixon-type sequences all produce four sets of images as shown below: water only, fat only, in phase, and out of phase. The fat-only images offer the potential for fat quantification. A minor disadvantage is an increase in minimum TR value (required to allow time for collection of the multiple echoes)

10.2.5 Dynamic Imaging of TMJ

10.2.5.1   Gradient Echo Imaging

Gradient echo (GRE) sequence, also known as gradient-recalled echo or fast field echo (FFE) sequences, uses gradient coils instead of a 180° refocusing RF pulse for producing an echo [3]. Frequency encoding is accomplished by applying gradients during data acquisition which are used to dephase (negative polarity) and rephase (positive polarity) transverse magnetization to create one or multiple echo signal [4]. In this sequence variable RF pulses (between 10° and 90°) also known as flip angle or tip angle are applied to create the transverse magnetization [20] (Fig. 10.11). After the α-degree RF pulse (characteristic flip angle), readout gradient is firstly applied with negative polarity and then reversed into positive polarity. This reversal of the gradients results in a regrowth of the signal and generates the echoes [5]. Since no 180° RF pulse is used, the main problem is the magnet inhomogeneities effect in this sequence. Depending on this technical characteristics, T2* dephasing with much shorter time than T2 occur in GRE [5, 20]. The most important advantage of the GRE sequence is short imaging time.
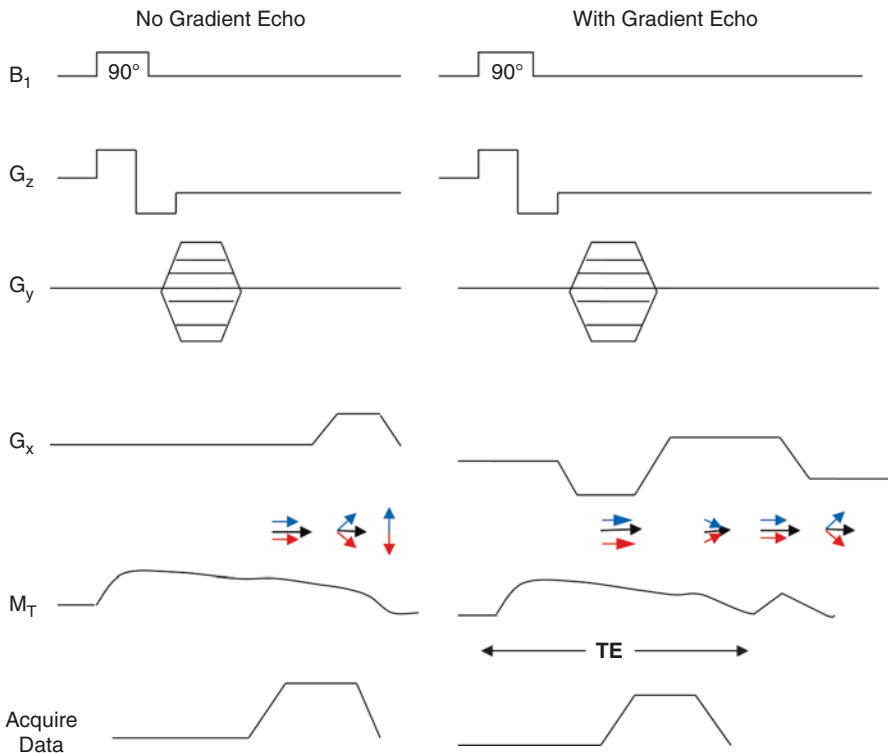

Fig. 10.11   Gradient echo pulse sequence formation diagram

T2* contrast affected by TE and T1 contrast is related with the flip angle and TR in this sequence. Larger flip angle and short TR introduces higher degree of T1 contrast, while lower flip angle and short TE accentuate T2* contrast [2, 3, 20]. Proton density contrast dominates when lower flip angle, longer TR, and shorter TE are used [2].

There are two broad categories of gradient echo sequences: incoherent gradient echo or gradient spoiled (spoiled residual transverse magnetization) and coherent gradient echo (refocused transverse magnetization). In the incoherent gradient echo sequence, the transverse magnetization is eliminated by a magnetic field gradient or a spoiler RF pulse.

A FFE sequence using a balanced gradient waveform. A balanced sequence starts out with a RF pulse of 90° or less and the spins in the steady state. Before the next TR in the slice phase and frequency encoding, gradients are balanced, so their net value is zero. Now the spins are prepared to accept the next RF pulse, and their corresponding signal can become part of the new transverse magnetization. Since the balanced gradients maintain the transverse and longitudinal magnetization, the result is that both T1 and T2 contrast are represented in the image. This pulse sequence produces images with increased signal from fluid, along with retaining T1-weighted tissue contrast. Because this form of sequence is extremely dependent on field homogeneity, it is essential to run a shimming prior to the acquisition. A fully balanced (refocused) sequence would yield higher signal, especially for tissues with long T2 relaxation times [20] (Figs. 10.12 and 10.13).

Fig. 10.12 An axial bFFE image of both TMJs showing increased signal from fluid (white arrow), along with retaining T1-weighted tissue contrast of the condyle (black arrow) and pterygoid muscle (arrow head)
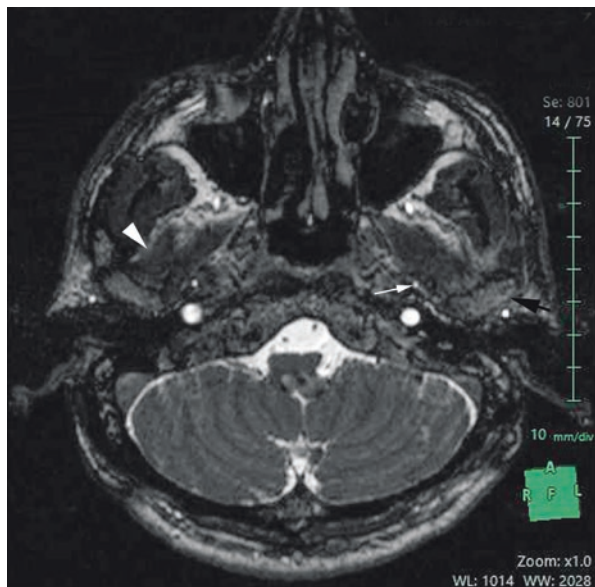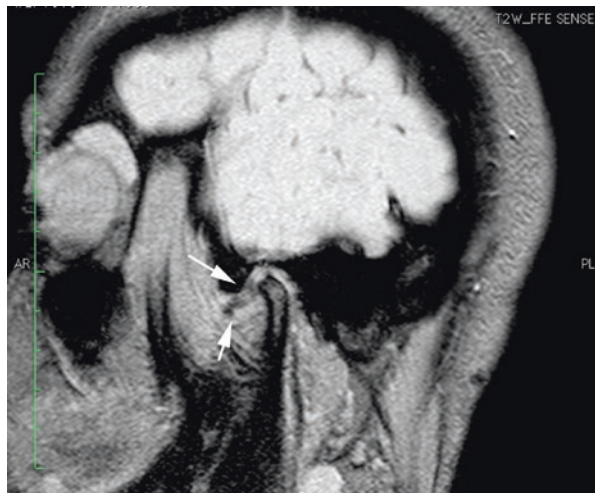
Fig. 10.13 A T2W-FFE image showing an anterior disc displacement without reduction case (arrows)

10.2.5.2   Echo Planar Imaging (EPI) Sequence

EPI allows ultrafast data acquisition (in 100–200 ms) and is performed by a series of gradient reversals in the readout direction [9]. EPI methods need strong and rapidly switched frequency-encoding gradients [3]. A gradient echo train is constituted by the application of the readout gradient continuously with positive and negative alternations [9]. If EPI sequence begins with the variable RF excitation pulse, it is called gradient echo EPI (GE–EPI), or if it begins with the 90° and 180° RF pulses, it is known as spin-echo EPI (SE–EPI). 180° refocusing pulse application needs for reducing artefacts caused by magnetic field inhomogeneities and chemical shift. SE–EPI has better image quality but longer scan time than GE–EPI [2].

10.2.5.3   Inversion Recovery (IR)

Inversion recovery pulse sequence is a variant of spin-echo sequence using the 180° inverting RF pulse to null or suppress the signal from certain tissues (e.g., fat or fluid). 180° RF pulse changes the direction of the nuclear magnetization from the positive z-direction into the negative z-direction. The regrowth of longitudinal magnetization starts to return the original orientation. After some relaxation occurrence process continue with the application of the 90° RF pulse. The time between the applications of the two RF pulses is called inversion time (TI) [3]. 90° RF pulse change the magnetization direction along negative y′ axis or the positive y′ axis depending on the inversion time used as an image contrast control [8]. Inversion recovery sequence provides heavily T1-weighted images which are primarily controlled by the TI value. A short TE application regarding to the T2 value decreases the T2 effect on IR sequence [20].

Two important clinical applications of the inversion recovery techniques are the short-tau inversion recovery (STIR) sequence and the fluid-attenuated inversion recovery (FLAIR) sequence [4].

Short-tau inversion recovery also known as short T1 inversion recovery sequence suppresses the tissue signal which has short T1 using a short IR [20]. Since the STIR sequence selectively suppresses the signal from fat, it provides excellent determination of the bone marrow edema [4] (Fig. 10.14).

FLAIR, a special inversion recovery technique, is used to null the signal from fluid (e.g., CSF, urine) using long inversion times. FLAIR sequence is very useful for evaluating the brain tissue [3, 4] (Fig. 10.15).

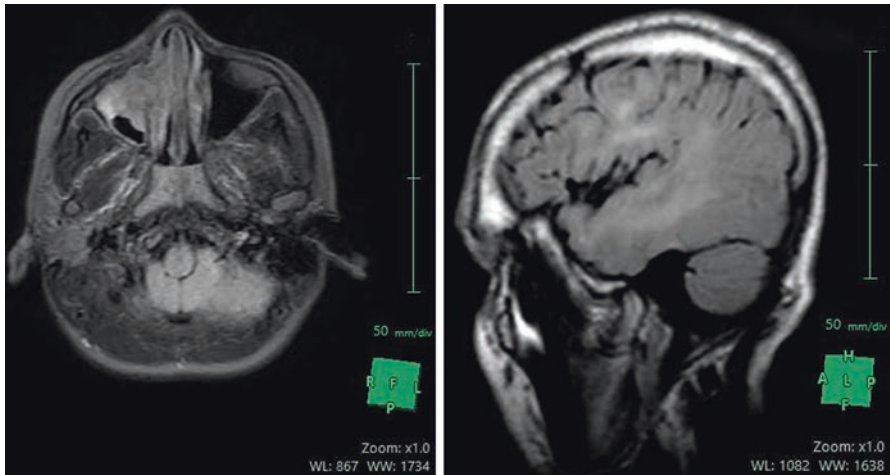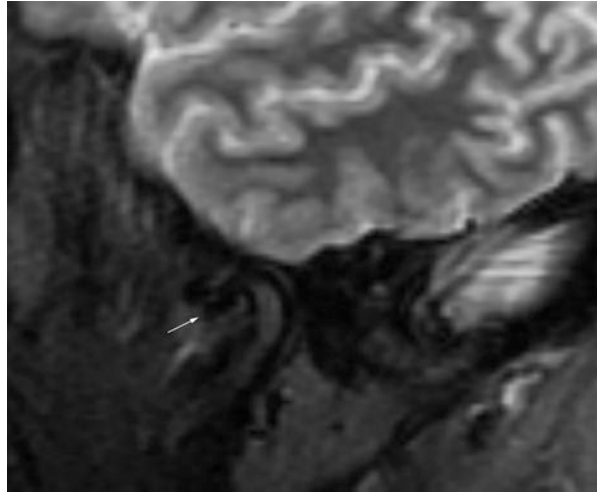**Fig. 10.14** Sagittal STIR image showing anterior disc displacement (arrow)

Fig. 10.15 Axial T1-W and sagittal T2W-FLAIR image showing TMJ structures. Note that the null is the signal from fluid

10.2.5.4 Half-Fourier Acquisition Single-Shot Turbo Spin-Echo (HASTE) Imaging

Half-fourier acquisition single-shot fast spin echo (HASTE) also known as single-shot fast spin echo (SSFSE) is a single-shot version of fast spin-echo which uses a single slice selective excitation and multiple refocusing RF pulses to reduce the number of phase-encoding steps with imaging times of 1 s or less [27]. Short acquisition time is an advantage to minimize the motion artifact and magnetic susceptibility [28]. Because a long time to repetition have to be selected to obtain an image in HASTE, sequence tissues with long TEs are well depicted, whereas tissues with short or medium TEs are not shown [3] (Fig. 10.16).

10.2.5.5 Steady-State Free Precession (SSFP)

SSFP is a highly effective unspoiled gradient echo sequence that accumulates signal from several echoes which are generated with repeatedly applied RF pulse. TR is usually kept as short as possible to minimize the acquisition time because SSFP sequences are very susceptible to artifacts caused by magnetic field inhomogeneities [4]. SSFP sequence image contrast is based on the ratio of T2/T1. Tissues which have high T2/T1 ratio appear bright, while tissues with a low T2/T1 appears dark on image. SSFP sequence is especially useful for evaluating the moving organs such as heart, vascular imaging [3], interventional MR imaging, and internal auditory canal in a short acquisition time with a high SNR [4].

GRASS (gradient-recalled acquisition in the steady state), FISP (fast imaging with steady-state precession), FIESTA (fast imaging employing steady-state

Fig. 10.16 Coronal T2W-HASTE image TMJ condyle on the right side
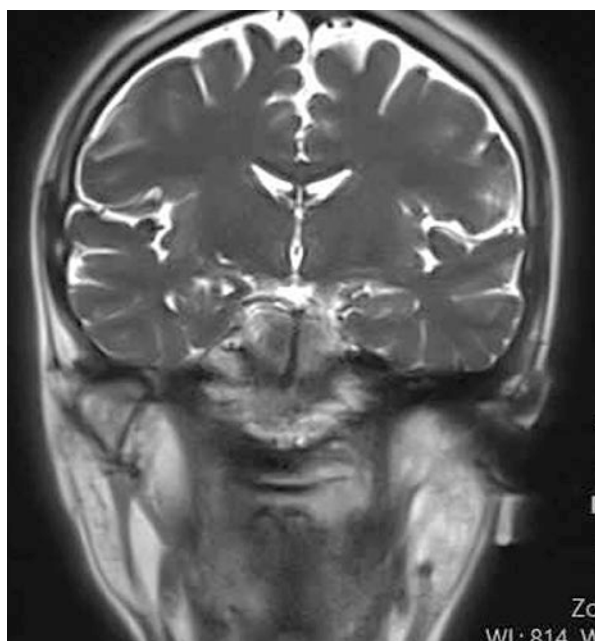
acquisition), balanced FFE (fast-field echo), and true FISP are the different names of the SSFP sequence depending on the manufacturers listed in Table 10.1.

Several studies used frequency-selective fat-saturated (FS) T2W sequence and found to be more sensitive than conventional T2W images in detecting marrow alterations and stated to be used instead of conventional T2W images [29–31], while the others used several sequences such as half-fourier acquisition single-shot turbo spin echo (HASTE) [32–34], fast low-angle shot (FLASH) [35, 36], and steady-state free precession (SSFP) (true fast imaging with steady-state precession (true FISP) [37], balanced fast field echo (bFFE), balanced turbo field echo (bTFE), and fast imaging employing steady-state acquisition sequence (FIESTA)24) especially for dynamic imaging of TMJ. Krohn et al. investigated the potential of real-time MR imaging (dynamic TMJ imaging) using 3T and concluded the advantage of 3T for this kind of imaging. Yen et al. developed an imaging protocol on a 3T system using the true FISP sequence that yielded an acceptable spatial and temporal resolution for dynamic MR imaging. In a recent study, used T2 mapping technique to evaluate TMJ disc ultrastructure. They concluded T2 relaxation time measurements could enable an ultrastructural analysis of the articular disc of the TMJ [38] (Fig. 10.17).

10.2.6 Advanced MRI Applications

10.2.6.1 Diffusion-Weighted Imaging (DWI)

Diffusion is the tendency of the molecules to move from a region where they are in high concentration to a region where they are in low concentration due to interactions with their surroundings. Two types of movement occur in tissues including coherent bulk flow and continuous movement in molecular space called as translational motion [9]. Diffusion is limited or restricted by various anatomical structures such as ligaments, membranes and macromolecules, as well as pathology. The net displacement of the molecules is named apparent diffusion coefficient (ADC) [2]. Diffusion constant in biological tissues may be measured by changing the b values (duration and interval of the gradients) with same imaging parameters [3]. If b value is zero, long TE and TR is resulted in T2W images; however, image weighting
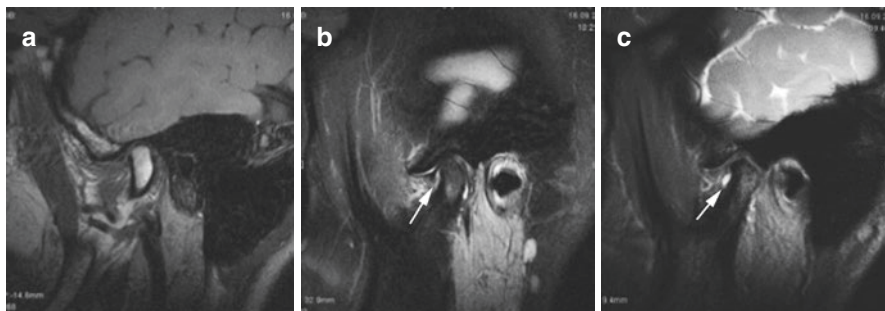

Fig. 10.17 (**a**) Conventional T2W image showing a normal bone marrow, (**b**) FS T2W, and 3D, (**c**) FIESTA-C sequences of the same patient demonstrated increased signal intensity with effusion in the inferior compartment of the joint and with the mandibular condyle bone marrow edema

changes into DWI when the b value (changing between the 500 and 1500 s/mm^2) increases [2]. ADC map is generated using the grayscale values which represent the mean ADCs of the corresponding voxels [3]. Pathologic tissues display high signal intensity on DWI and is characterized by lower ADC value than normal tissue due to the restriction of the diffusion when pathology is present [2].

DWI is very useful for evaluating the cholesteatoma, assessment of the malignant tumors, prediction and monitoring of treatment response, and differentiation of recurrent tumor from posttherapeutic changes in head and neck cancer [39] (Figs. 10.18 and 10.19).

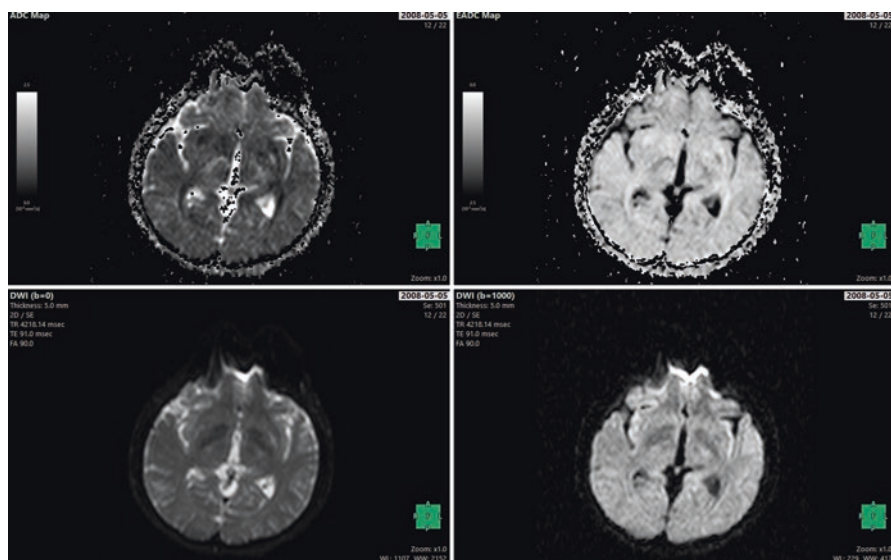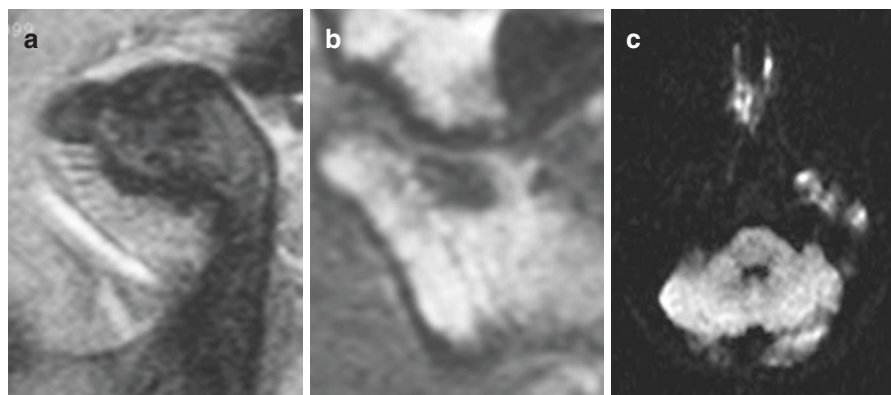**Fig. 10.18** DWI images showing ADC map, EADC map, b = 0, and b = 1000 images

Fig. 10.19 (**a**) t1-W, (**b**) T2-W, and (**c**) diffusion-weighted images at b value1000 showing non-restricted diffusion in an osteochondroma case of the TMJ condyle

10.2.6.2   Perfusion-Weighted Imaging

Perfusion is a relative and/or absolute measurement of the parameters of regional blood flow, vascular supply to a tissue, and tissue activity [2]. Perfusion-weighted imaging is of great help to evaluate the microvascular blood flow in the brain, the myocardium, the lungs, the spleen, and the kidneys [2, 3]. This technique relies on the use of a tracer either a bolus injection of exogenous perfusion contrast agent such as gadolinium or endogenous saturating the protons in arterial blood with RF inversion or saturation pulses [2]. A paramagnetic contrast agent application results in a shortening of both longitudinal and transverse relaxation times, visceral with high perfusion appear as an increase in signal on T1-weighted images and a decrease on T2- or T2*-weighted images [2, 3]. (Figs. 10.20 and 10.21).

10.2.6.3   High-Speed Real-Time Radial FLASH MRI

Real-time MR imaging of moving spins focuses on the observation of dynamic processes such as tongue movement, cardiac imaging, and fetal imaging. This technique is based on acquisition of dynamic images in a short period of time. In order to achieve dynamic images, specific reconstruction algorithms should be used in order to constitute the MR images. FLASH sequence is one of them that can be used with regularized nonlinear inversion for achieving real-time phase-contrast imaging [40].

Fast low-angle shot (FLASH) is the most commonly used spoiled gradient-echo MRI sequence. FLASH uses radio-frequency excitation pulses with a low flip angle (less than 90°) and subsequent reading gradient reversal for producing a gradient echo signal. The small flip angle pulses create equilibrium of longitudinal magnetization. Transverse magnetization is eliminated by a strong gradient (spoiler gradient). T1-weighted and T2*-weighted contrast can be set with the FLASH sequence. In comparison to spin echo, FLASH is more sensitive to field inhomogeneities and susceptibility differences. On the other hand, it provides several advantages such as reduction in acquisition time due to short TR, lower specific absorption rate, and extra contrast due to imaging at in-phase and opposed-phase conditions [41, 42].

For FLASH imaging, due to transverse magnetization in steady state, there are three types of FLASH sequences such as spoiled, refocused FLASH, and balanced steady-state free precession (bSSFP). Spoiled FLASH employs RF spoiling or gradient spoiling to destroy the transverse magnetization. Gradient spoiling involves the application of the gradient pulses which results the dephasing of the residual magnetization [43]. For radial spoiled FLASH, the technique itself employs a fast low-angle shot sequence with proton density, T1 or T2/T1 contrast, and radial data encoding for motion robustness. High temporal resolution is achieved by an up to 20-fold undersampling of the radial data [41, 43, 44].

Radial views are acquired in a certain view order to fill the k-space. The simplest method fills the k-space in which the order plays a major role in dynamic imaging as the motion of the object. The distribution of radial views in k-space and different types of view order had been studied extensively [40]. The sequential reordering
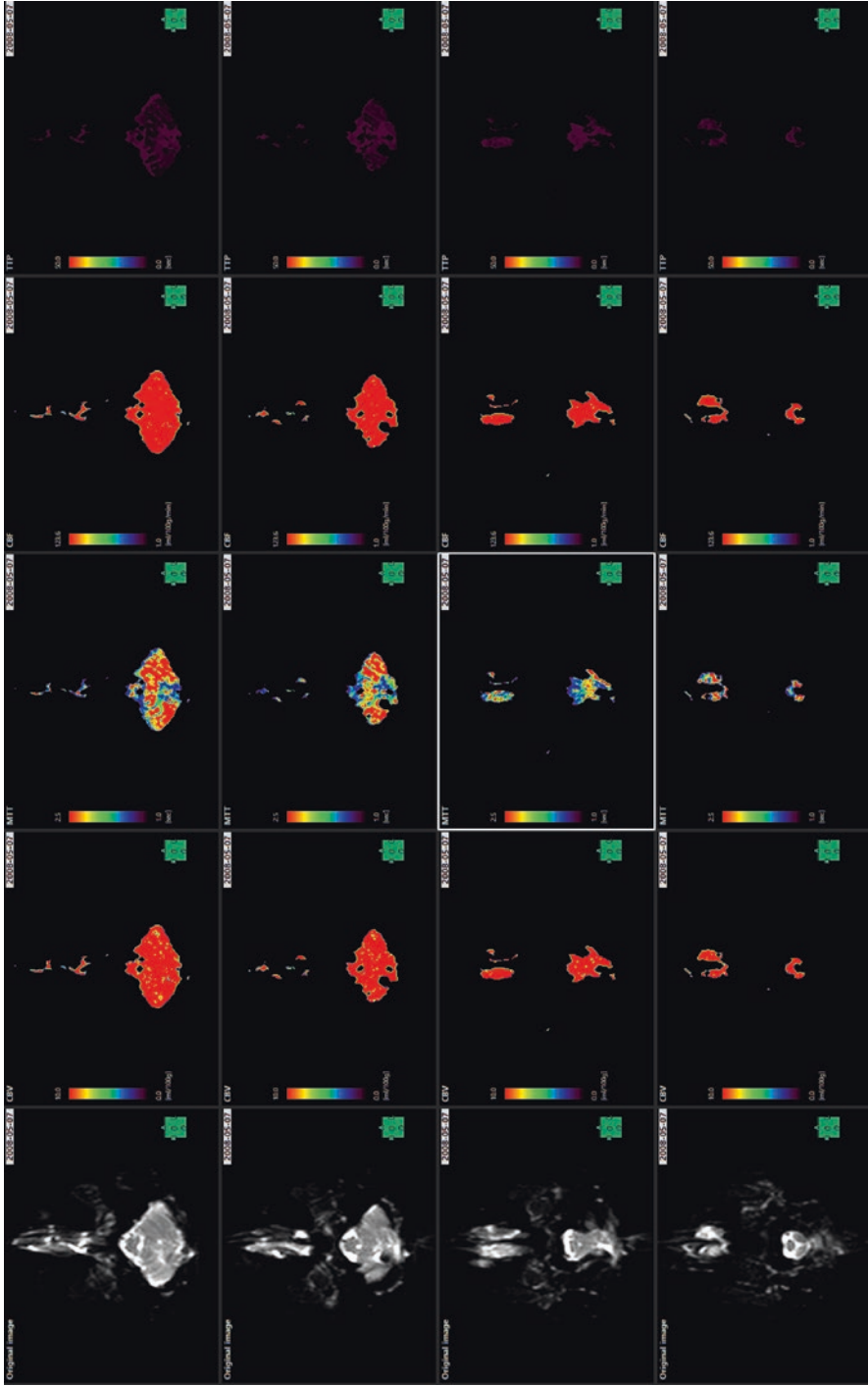
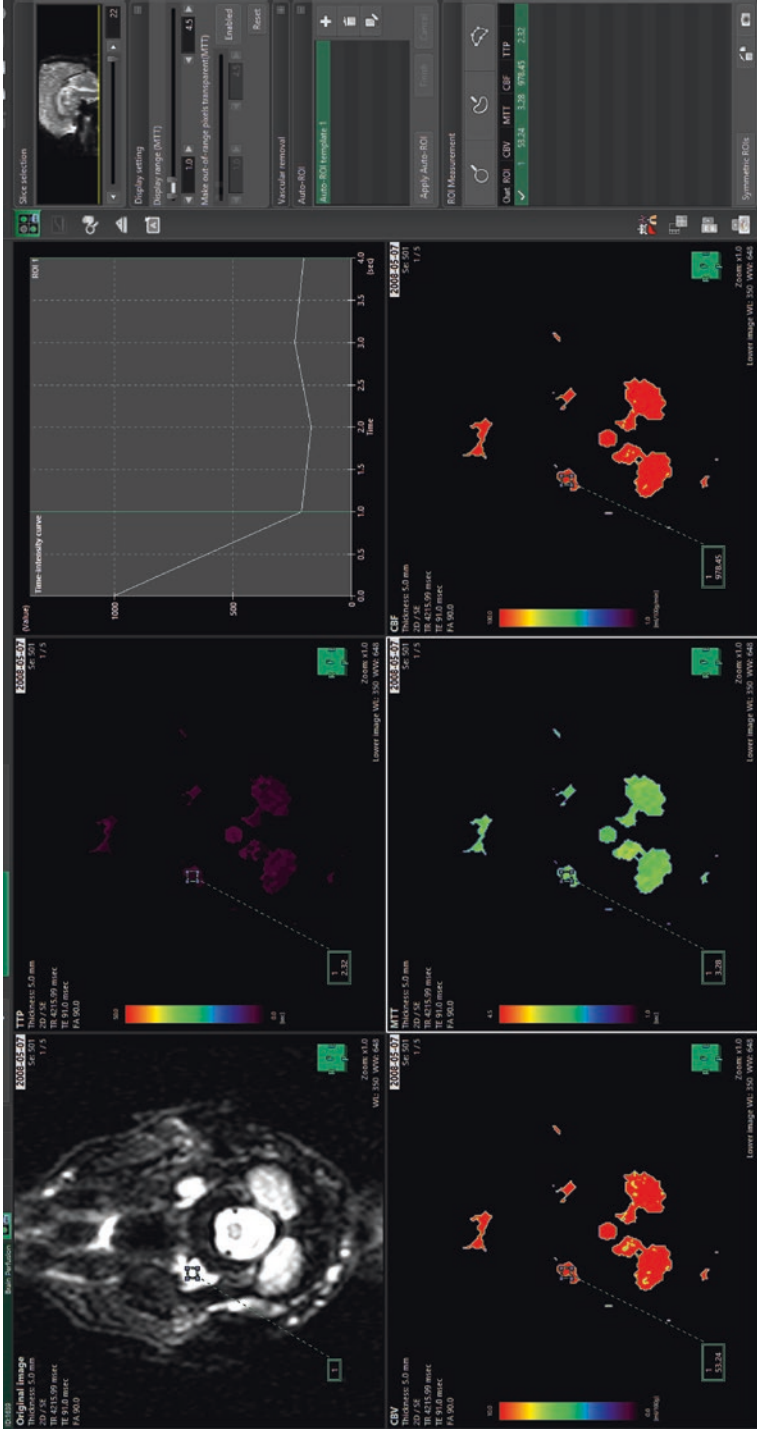**Fig. 10.20** MR perfusion study showing blood flow parameters

Fig. 10.21 MR perfusion study describes rate and level of blood flow (CBF) to tissues with time–intensity curve

scheme along with five radial turns was experimentally found to be optimal for dynamic imaging.

However, in this technique, the obstacle is the coil sensitivity esp. in parallel and real-time MRI due to short acquisition time. If the receive coil sensitivities are known, the image recovery an efficiently be solved using iterative methods. In practice, however, static sensitivities are obtained through extrapolation, and in a human subject during any type of movement (e.g., breathing or TMJ imaging) or when dynamically scanning, different planes and orientations (e.g., during real-time monitoring of minimally invasive procedures) can be effected dramatically. In such situations, extrapolating static sensitivities is not sufficient and thus should be corrected with various reconstruction algorithms [44, 45].

Increasing imaging speed is of utmost importance in in vivo MRI and can be simultaneously acquire several slices of an object, which allows for higher undersampling factors compared to single- or conventional multi-slice measurements by exploiting axial coil sensitivity information. Furthermore, these MRI benefits from an inherently increased SNR which contributes to an improved overall image quality. For real-time dynamic MRI changes during a physiologic process, there is need for undersampled data sets which can be solved with nonlinear inverse problem. Simultaneous multi- slice (SMS) MRI together with reconstruction techniques such as regularized nonlinear inversion (NLINV) formulates the image reconstruction as a nonlinear least-squares problem for dynamic imaging [46].

This approach has been tested for high spatial MRI, in particular MRI studies for articulation [47], brass playing [48] to swallowing [49, 50], etc. Although there are a couple of studies, so far no detail imaging was done for TMJ FLASH imaging. The easy way to recognize the FLASH images is to check for fluid-filled space around TMJ area (e.g., cerebrospinal fluid, synovial fluid in the joint). Fluids normally appear as dark on a FLASH image (Fig. 10.22). However, the application for TMJ is still not tested in detail for this imaging sequence and reconstruction.
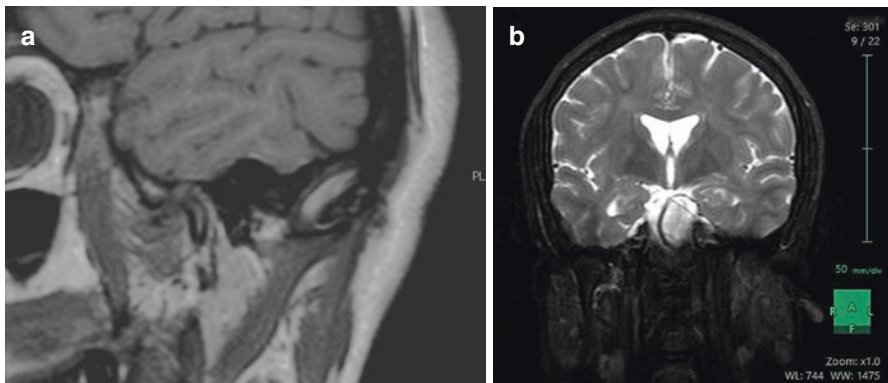

Fig. 10.22 (**a**) T1-W flash and (**b**) T2-W FLASH sequences. Note that the easy way to detect FLASH images is to check for fluid the filled space which fluids normally appear as dark

10.3   Contrast Media and Contrast Enhancement

Image contrast in medical MR imaging is due to differences in signal intensity (SI) between the two tissues [3]. Since the earliest stages of development of this imaging modality, contrast enhancement media have been used for magnetic resonance imaging. The contrast agent used in computerized tomography and magnetic resonance imaging is working with completely different mechanism. The contrast agent used in computerized tomography accumulates in the tissue and visualized with the ability to absorb X-ray photons. On the other hand, the contrast agent used in magnetic resonance imaging indirectly functions with changes in the local magnetic environment [51]. The contrast agent used in this imaging is pharmaceutical preparations applied in MR imaging to further enhance natural contrast and also to obtain dynamic (pharmacokinetic) information. To achieve these goals, the contrast agents used for MRI must have certain physicochemical properties as well as a suitable pharmacokinetic profile.

The MR contrast medical changes its contrast properties of biological tissues in two basic ways.

– Directly by changing the proton density of a tissue or
– Indirectly, by altering the local magnetic field and the resonance properties of a tissue and thus the T1 and/or T2 values [3]

The use of contrast media enhances the sensitivity and specificity of the MRI sequences by chancing the intrinsic properties of tissue depending on the tissue vascularity, capillary permeability, and extracellular fluid volume following oral or intravenous administration [52, 53]. There are several different contrast agents available for MR imaging. Some of the contrast materials used in magnetic resonance imaging are gadolinium-based, while others include gadolinium-free materials. Gadolinium (Gd)-based chelates entering clinical use in 1998 represent the basis of intravenous contrast-enhanced MR imaging [54]. This Gd chelates are highly water soluble and contain Gd ion. Gadolinium is an earth metal which has special paramagnetic properties, making it useful as a contrast agent for MRI scans. The paramagnetic properties of this contrast agents result from the numerous unpaired electrons that exist within its inner shells. These unpaired electrons can interact with adjacent resonating protons and cause the protons to relax more rapidly. This result in a shortening of both longitudinal and transverse relaxation with consequent reduction in the T1 and T2 values of the tissue in which it accumulates [52, 53]. This is depicted as an increase in T1-weighted image and a decrease in T2-weighted image signal. In practice, the signal increase detected on T1-weighted imaging is better appreciated than any corresponding signal decrease in T2-weighted imaging and makes T1-weighted imaging the method of choice for intravenous contrast studies [55]. Fat suppression is often used to suppress the high signal from fat and obtain a reliable acquisition of contrast material-enhanced images [52].

Gadolinium-based contrast agents (GBCAs) are used to enhance the image approved by the Food and Drug Administration (FDA) including Ablavar (gadofosveset trisodium), Dotarem (gadoterate meglumine), Eovist (gadoxetate disodium), Gadavist (gadobutrol), Magnevist (gadopentetate dimeglumine), MultiHance

(gadobenate dimeglumine), Omniscan (gadodiamide), OptiMARK (gadoverset-amide), and ProHance (gadoteridol).

The standard dose of extracellular contrast material administration shortens T1, which leads to an increase in signal intensity in vessels and tissues due to tissue perfusion or disruption of the capillary barrier (brain, spinal cord, eyes, testes). The extracellular contrast medium is administered intravenously as a bolus or drip infusion at a dose of 0.1–0.3 mmol/kg body weight. In MR angiography, higher doses were administered consecutively up to 0.5 mmol/kg body weight [3]. The major elimination pathway of these agents is through glomerular filtration and renal excretion. Half-life is usually 90 min, but it takes 24 h for complete elimination of the agents. Contrast agents used in MR imaging have several advantages over those used in CT. CT agents are direct agents; they contain an atom (iodine, barium) that attenuates or scatters the incident X-ray beam, differently from the surrounding tissue. This scattering permits direct visualization of the agent itself regardless of its location. Most MRI contrast agents are indirect agents and never directly visualized in the image, affecting the relaxation times of water protons in nearby tissues. The incidence of side effects due to MRI agents is very low, as the concentration and dosage of MRI contrast medium is significantly lower compared to CT [9].

Gadolinium contrast agents are considered to be safer than the nonionic iodinated contrast material. Gadolinium contrasting substances are less reactive than iodized substances, and most of them are minor and self-limiting [56]. European Society of Magnetic Resonance in Medicine and Biology (ESMRMB) classified adverse reaction to gadolinium-based contrast agent (Gd-CA) into the four groups [57]. The vast majority of these reactions are mild, including coldness at the injection site, nausea with or without vomiting, headache, warmth or pain at the injection site, paresthesias, dizziness, and itching. Reactions resembling an "allergic" response are very unusual and vary. A rash hives, or urticaria are the most frequent of this group, and very rarely there may be bronchospasm. Severe, life-threatening anaphylactoid or nonallergic anaphylactic reactions are exceedingly rare. Fatal reactions to gadolinium chelate agents occur but are extremely rare. Gadolinium chelates administered to patients with acute renal failure or severe chronic kidney disease can result in a syndrome of nephrogenic systemic fibrosis (NSF) [57].

Contrast media application is resulted in some adverse reaction in very rare cases, and frequency of the anaphylaxis or allergic-like reactions is less than 0.5% of patients [58, 59]. Late side effect reactions occur between 1 h and 7 days after administration of intravascular iodinated contrast media [60]. The most commonly identified symptoms in acute minor reactions include flushing, nausea, arm pain, pruritus, vomiting, headache, and mild urticaria [61]. Most of the reactions are self-limited, and up to the three-quarters resolve within the first 3 days and others in 7 days. Serious late reactions have been reported that require treatment at the hospital, permanent disability, or even death; however, it is very rare [60].

Nephrogenic systemic fibrosis (NSF) is a potentially debilitating disease. The exact pathogenesis of nephrogenic systemic fibrosis is uncertain, but the disease has been associated with the use of gadolinium-based contrast agents in patients with predominantly acute renal failure or end-stage renal disease [62]. The time between the initial NSF-eliciting gadodiamide exposure and the appearance of the first symptom is commonly referred to as the symptom-free, or asymptomatic period may extend from 0 to 53 days with an average of 2 weeks [63]. In most of the NSF patient,

skin involvement is the initial symptom that begins with the swelling in the distal parts of the extremities [64]. Whereas some of the NSF patients have symptoms such as leg pain and swelling, pneumonitis, and diarrhea appearing more acutely within less than 24 h, the others may have more chronic symptoms like contractures that firstly appear up to 2 months. Skin thickening may be aggressive and in relationship with persistent pain and loss of elasticity in the skin and muscle. In some patients NSF may progress to physical disability, whereas some of them need to use wheelchair. In some patients, skin thickening results in contractures with the inhibition of flexion and extension in the joints [63]. The severity of the disease is directly proportional to the amount of the drug or contrast agent, but there is an exposure limit required for the patient to show the symptoms. Disease can occur even at lower doses if the agent is given over a specific dose or if the patient is susceptible to the agent. In order to prevent this disease, in MRI, it is important to choose the substance that releases least gadolinium in the body and to ensure that the agent has high stability and relaxation [65].

10.4 Image Artifacts

Artifacts are one of the most important handicap of MR images. An artifact is defined as a distortion in MRI signal intensity with no identifiable anatomical source in the imaging field.

Artifacts can be categorized in many ways; the first group is a consequence of motion of patient tissue during the measurement. The second group is produced primarily as a result of the particular measurement technique and/or specific measurement parameters. The last group is independent of the patient or measurement technique; it occurs because of the malfunction of the MR, external source, or the scanner during shooting [9].

Routine MR imaging usually involves two types of motion artifacts:

– With respiratory, peristalsis, or from the beating heart
– Pulsatile blood flow or cerebrospinal fluid (flow artifacts) [3]

Patient motion during the acquisition of a magnetic resonance image can cause blurring and ghosting artifacts in the image [66]. These movement artifacts also appear to be an antagonistic problem in other examination methods; however, the duration of the examination in MRI is longer than the other imaging techniques, which causes the artifacts to become apparent. In addition, because the routine examinations are carried out with the multi-slice technique, the motion within the examination period reflects many interactions in our examination plan. Basically, the artifact is caused by the encoding of the signal from the tissue into the wrong voxels during the frequency-coding and phase-coding gradients or by multiple coding of the same voxel. Cardiac, respiratory movements, vascular pulsations, CSF pulsations, periodic or intestinal peristalsis, and swallowing like physiological movements of the patient lead to significant artifacts in the image. The most commonly used method to remove artifacts that are caused by periodic movements today is the "physiological gate" technique (cardiac gating, breathing gating). This means that the signal is recorded only in one phase of these physiological periodic movements [1].

10.4.1 Aliasing Artifacts

Wrap or aliasing produces an image where anatomy that exists outside the FOV is folded onto the top of anatomy inside the FOV [2]. This artifact is often seen on the phase-coding or frequency-coding axis or both axes when the region under examination is smaller than the patient volume or when working with a small FOV [1]. Aliasing artifact can be reduced or eliminated by increasing the FOV, changing the gradient axes relative to the patient, and displaying only the central portion of the actual FOV, use of surface coils, or inner volume imaging techniques [67].

10.4.2 Chemical Shift Artifact

The chemical shift phenomenon refers to the signal intensity alterations seen in MR imaging that result from the inherent differences in the resonant frequencies of precessing protons [68]. Hydrogen is our target in MR images. This makes the water our target. But the oil also contains hydrogen and carbon to generate the signal. They also generate a lot of signal. We often see chemical shift artifacts as dark and shiny lines at the water and oil boundary.

10.4.3 Out-of-Phase Artifact

This is also called chemical misregistration. This artifact is caused when the precession of fat and water are out of phase. When hydrogen protons in fat and water are in phase within a pixel, the signal is produced in these tissues. When fat and water hydrogen protons are out of phase within a pixel, no signal is produced. This will be represented as a dark signal boarder around organs [2].

10.4.4 Zipper Artifact

Zipper artifacts are common in conventional MR imaging and originate from contamination of the nuclear MR imaging signal by spurious radio-frequency (RF) noise, a result of either a compromised faraday cage or faulty equipment within the scanning room [69]. A conventional zipper artifact appears as one line or a series of alternating black and white lines, giving the artifact its name. Because a zipper artifact results from a set of contaminant RFs, it fills one or more lines in the image at a given location along the frequency-encoding axis [69, 70]. In parallel MR imaging, zipper artifacts appear along the frequency-encoding axis. The RF noise also leads to reconstruction errors in the form of a subtle ghost that can overlap with areas beyond the zipper artifact. If not severe, a zipper artifact may not prevent interpretation of conventional MR images, which may cause the origin of the artifact to be ignored.

Depending on the source, RF noise and the subsequent zipper artifact may disappear and reappear at different times during the examination. First, a zipper may be visible in the image itself. Reconstruction programs recognize zippers as anatomy that should be present in the sensitivity map. Second, in addition to being seen on

images, a zipper may appear during calibration scanning, which leads to a faulty sensitivity map. Both cases may lead to problems in reconstruction. In the second case, differences between calibration and imaging protocols, such as bandwidth and pulse sequence timing, change the position and appearance of zipper artifacts [69].

10.4.5 Magnetic Susceptibility Artifact

Magnetic susceptibility artifacts are the result of microscopic gradients of the magnetic field strength at the interfaces of regions of different magnetic susceptibility. Paramagnetic materials such as platinum, titanium, and gadolinium have positive susceptibility and augment the external field. Diamagnetic substances (water, most biological substances) have negative susceptibility and slightly weaken the external field. Ferromagnetic materials (iron, cobalt, nickel) have strong nonlinear positive susceptibility. There are two main effects of magnetic susceptibility [71]. First, ferromagnetic materials can lead to a strong distortion of the B_0 field and the linearity of the frequency encoding gradient close to the object. This frequency shift results in geometric distortion of the image. Second, susceptibility gradients result in different precession frequencies of adjacent protons, resulting in stronger dephasing of spins. The net results are bright and dark areas with spatial distortion of surrounding anatomy. Lightweight reduction of artifact may also be achieved using wide broadband width techniques that enhance gradient strength [70].

10.4.6 Herringbone Artifact

A crisscross or herringbone artifact is due to a data processing or reconstruction error. It is characterized by an obliquely oriented stripe that is seen throughout the image. These artifacts can usually be eliminated by reconstructing the image again [3].

10.4.7 Truncation

This artifact is also known as "ringing artifact" or "Gibbs phenomenon." It is usually seen along the phase-encoding axis and in 128 phase-encoding step numbers (such as matrix 128 × 256). This artifact occurs in Fourier transformation, and it is not possible to perform signal sampling for the required time for the image. This artifact is often lost when using 256 phase-coding step numbers. Therefore, to avoid this artifact, the number of phase-coding steps can be increased, or the frequency-coding gradient axes can be shifted by phase coding [1, 70].

10.4.8 Shading Artifact

The signal intensity of each voxel is directly related to the radio frequency in that region. When the transmitter or receiver coil generates an unequal radio-frequency field, the signal intensity will not be equal. This artificial object is intimate in all

views of the spinal column obtained with a surface bobbin because the radio-frequency field is significantly reduced from the bobbin; this significant reduction causes a gradual loss of image brightness. This type of artifact is eliminated by breaking the loop and thereby preventing the induction of eddy currents [72].

10.4.9 Partial Volume

Partial volume artifact occurs when a voxel signal represents an average of different tissues, which results in a loss of resolution. To avoid this artifact, thinner slices should be chosen, but this can lead to a poor SNR [70].

10.4.10 Artifacts Due to Metal

Artifacts caused by dental restorations, such as dental crowns, dental fillings, and orthodontic appliances, are common problems in MRI and CT scans of the head and neck. The presence of ferromagnetic metals in some dental materials causes magnetic field homogeneity, where metal-based materials form their own magnetic fields and dramatically alter the frequency of pressing the protons in adjacent tissues. The tissues adjacent to the ferromagnetic components are influenced by the induced magnetic field of the metal, so either a different frequency precipitates or fails, thus not producing a useful signal [73].

Surgical implants: The knowledge about the amount and distribution of artifacts through different implant materials in various image modalities and settings might help support the decision for choice of implant material in the clinical setting, accounting for the image modality needed for future diagnostic or monitoring purposes. Within the limits of the current in vitro study, zirconium implants are the most suitable for MRI, and only minimal artifacts are exhibited, especially in the T1W series, without a significant reduction in image quality. Corresponding titanium and titanium zirconium alloy implants exhibit large artifacts on both T1W and T2W images, leading to a reduction in diagnostic image quality near the implant [74].

Orthodontic devices (e.g., fixed or removable orthodontic and maxillofacial orthopedic devices) constitute the major portion of metal artifacts among other metallic dental objects such as metal crowns and titanium implants with regard to the extent of artifact in MRI. Various orthodontic brackets are available in market in terms of texture including stainless steel (SS), ceramic, ceramic with SS slots, plastic, and titanium brackets [75]. Not all the brackets should be removed before the MR imaging, and particular decision should be made individually considering the area of interest to be studied and type of brackets worn. It has been shown that 3M orthodontic brackets, in combination with NiTi wires in particular, cause smaller signal-free zones. In general, it is known that 3M and Dentaurum orthodontic brackets with NiTi wires generate less artifacts than SS braids with the same brackets. When nickel-free orthodontic brands are compared to nickel-containing brands, the effect on the size of the signal-free zones is not significant [76] (Fig. 10.23).
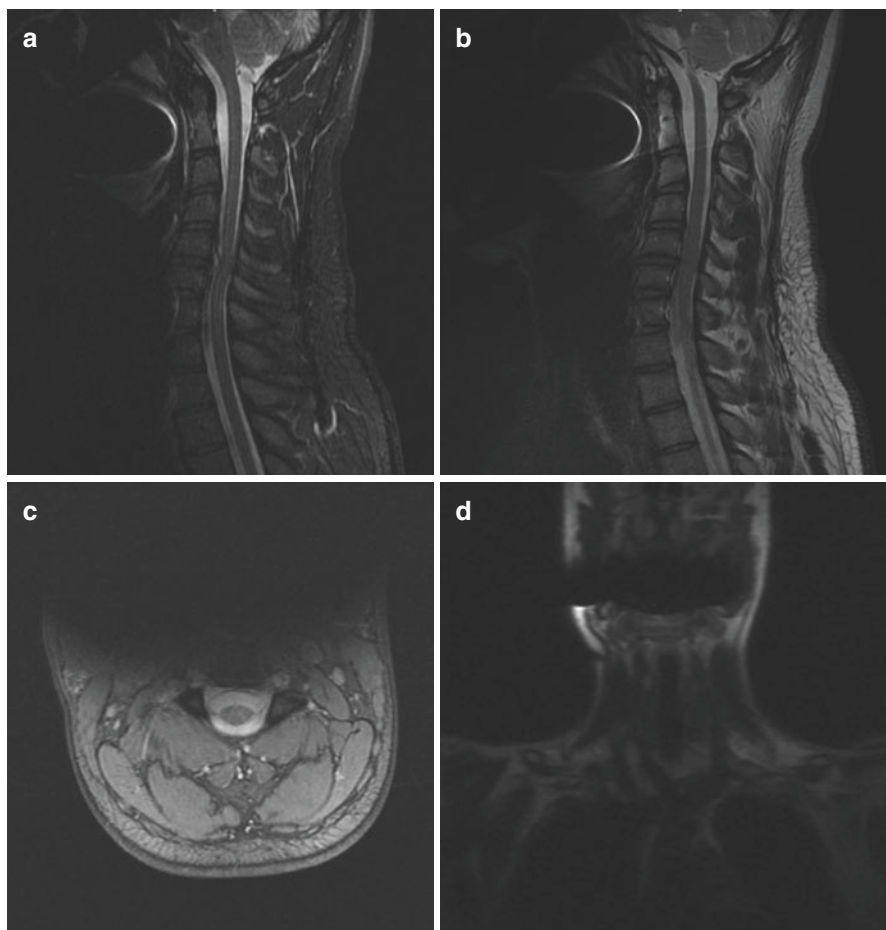
Fig. 10.23 (**a**) STIR, (**b**) T2-W, (**c**) MERGE, (**d**) coronal T1-W image showing artifact due to orthodontic bracelets' and wires

10.5 Contraindications for the Procedure

10.5.1 Metallic Implants and Vascular Clips

If a clip is made of non-ferromagnetic material and there is no concern with MR-associated heating, a patient may undergo MR immediately after implantation [77]. If the clip is made of titanium or titanium alloy, MR imaging can be done. However, if the clip is declared to be ferromagnetic or otherwise incompatible with MR, the examination must be canceled [78].

10.5.2 Foreign Bodies

If there is any doubt about the presence or location of foreign bodies, an X-ray should be taken before the MRI. The same holds true for bullets or grenade fragments. Shifting of metal foreign bodies under the influence of the magnetic field could damage vital structures such as vessels or nerves [79]. The most widely used types in clinical practice have been tested at magnetic fields of 1.5 T and 3 T and were found to be safe for MRI [78].

10.5.3 Coronary and Peripheral Artery Stents

Most coronary artery and peripheral vascular stents are made of stainless steel or nitinol. Some stents may contains variable amounts of platinum, cobalt alloy, gold, tantalum, MP35N, or other materials. That means most coronary and peripheral vascular stents are non-ferromagnetic or weakly ferromagnetic [80]. Extensive studies have led to the conclusion that MR scanning of patients after stent implantation can be performed without risk at any time at 3 T or less. However, stents generally cause artifacts that impair evaluation of the stent itself [77].

10.5.4 Prosthetic Heart Valves and Annuloplasty Rings

Although prosthetic heart valves and annuloplasty rings are made from a variety of materials, numerous studies have demonstrated that MRI examinations are safe. Even mechanical heart valves that are composed of a variety of metals are not contraindicated for MR imaging at 3 T or less any time after implantation. Depending on the amount of metal contained, there are some minor interactions with the magnetic field, but the resulting forces are much less compared to those of the beating heart and pulsatile blood flow. Sternal wires are usually made of stainless steel or alloy and are not a contraindication to MRI [78].

10.5.5 Inferior Vena Cava Filters

Many inferior vena cava filters are made of nonferromagnetic materials, whereas some others are composed of weakly ferromagnetic materials. Devices such as inferior vena cava filters are attached with hooks. As is typical for healing processes throughout the body, it is generally believed that inferior vena cava filters become incorporated securely into the vessel wall, primarily due to tissue ingrowth, within 4–6 weeks after implantation [81]. Therefore, it is unlikely that such implants would become moved or dislodged as a result of exposure to static magnetic fields of MR systems operating at up to 1.5 T [78]. Studies of MR examination of both animals and humans with implanted inferior vena cava filters have thus far not reported complications or symptomatic filter displacement [81].

10.5.6 Permanent Cardiac Pacemakers and Implantable Cardioverter Defibrillators

It has been estimated that a patient with a pacemaker or implanted defibrillator has a 50–75% likelihood of having a clinical indication for MR imaging over the lifetime of their device. These devices contain metal with variable ferromagnetic qualities, as well as complex electrical systems [77]. The real danger for pacemaker patients undergoing MRI examination is competitive rhythm in the case of asynchronously pacing generators and spontaneous, sometimes tachyarrhythmic heart rhythms. It is neither inhibition of the pacemaker nor heating of the lead tip that poses a real risk. Patients with magnet function off can safely be examined, if scanning is restricted to the refractory period of the pacemaker. Patients with non-programmable magnet function can be examined only if spontaneous beats are absent. Patients with asynchronous pacing and tachyarrhythmias should be handled in a special way, either by careful monitoring with a defibrillator at hand or by programming the output parameters to below threshold. Pacemakers with programmable magnet function should preferably be implanted, for the benefit of patients who may later require MRI examination [82].

10.5.7 Permanent Contraceptive Devices

Contraceptive devices have been tested for MR imaging safety, including intrauterine devices (IUDs) and contraceptive diaphragms. IUDs may be made entirely of nonmetallic materials, such as plastic, or a combination of nonmetallic and metallic materials. Typically, copper is the metal used in IUDs [83]. Therefore, heating and displacement might be the consequence of MRI. However, the results of various studies indicate that these devices are safe when patients are examined using magnets of 1.5 T or less. It is a general recommendation to inform the patient that displacement of the device might have occurred following the procedure, with consequently inappropriate anti-contraceptive effects. Therefore, the correct position of the device should be checked by ultrasound after the intervention [78]. The metallic component of an IUD may cause artifacts; however, such artifacts are relatively minor because of the low magnetic susceptibility of copper and relatively small size of the IUD [83].

10.5.8 Cochlear Implants

Cochlear implants are mechanical devices used for patients with severe sensory-neural hearing loss, which has an inner magnet [84]. These systems consist of complex electric and metal components. Various systems are in use, and the implantation numbers are increasing. This makes the compatibility of cochlear implants with MRI an increasingly relevant topic. Numerous devices have been tested for MRI safety. In general it is most important to know precisely which implant is present and the intended MRI procedure. Force and torque induced by the magnetic field of

the MRI represent a hazard for the implant. Thus, cochlear implants represent a relative contraindication to MRI, and only after careful evaluation of the individual risk can an MRI possibly be performed [78].

10.5.9 Other Potential Contraindications

10.5.9.1   Tattoos and Cosmetics

Both tattoos and cosmetics may contain particles of iron oxides or other metals that, by interacting with the magnetic field, can cause sensations of heat, burns, swelling, or local irritation during an MRI examination [85]. If possible cosmetics should be removed before scanning. The same holds true for piercing material. If removal is not possible, an icepack/cold compress may be used. In a review of the literature, Shellock and Crues conclude that neither tattoos nor cosmetics are a contraindication for MRI, provided that appropriate precautions are taken [86].

10.5.9.2   Claustrophobia

Claustrophobic reactions happen in 1–15% of all patients who undergo an MR examination and consequently cannot be imaged or require sedation. The extent of claustrophobia is very variable and depends on the type of scanner, position in the scanner, gender, and age. When a patient reports that he or she is suffering from claustrophobia, it has to be taken seriously; besides the possible option of sedating the patient, the incidence of claustrophobia can be reduced by a factor of three by using recently developed scanners with a conical-shaped short magnet bore and reduced acoustic noise [78]. Oral benzodiazepines, prism glasses, communication devices, having a relative or friend present in the room, and music are other long-established options to reduce claustrophobic responses to MR examinations [87].

10.5.9.3   Pregnancy and Postpartum

Diagnostic imaging might be required during pregnancy for several reasons. MR procedures have been used to evaluate obstetric, placental, and fetal abnormalities in pregnant patients for more than 18 years [86]. The existing safety issues are related to possible adverse biological effects by the magnetic fields. MRI may be used in pregnant women if other non-ionizing forms of diagnostic imaging are inadequate or if the examination provides important information that would otherwise require exposure to ionizing radiation (e.g., fluoroscopy, computed tomography). If the diagnostic information outweighs concerns about potential negative effects clinically, the MRI examination can be performed with oral and written informed consent provided [78].

10.5.10 MRI and Contrast Agent

10.5.10.1   Paramagnetic Contrast Media During Pregnancy
and Breast-Feeding

Although gadolinium containing contrast media cross the placental barrier, no published data of teratogenic or mutagenic effects on the fetus related to the

administration of gadopentetate dimeglumine, gadoteridol, gadobenate, dimeglumine, or gadoversetamide in pregnant women exist [78].

Paramagnetic contrast media are filtered and eliminated by the kidneys; however, the mammary gland can also contribute to their excretion to a small extent, and so breast milk may contain an extremely small amount of contrast medium. With the data demonstrating the safety of intravenous and oral gadolinium-containing contrast agents in infants and the low amounts of gadolinium found to be excreted in human breast milk, it is timely to reconsider the justification for a 24 h precautionary suspension of breast-feeding following gadolinium containing contrast agent administration. The need for a 24-h suspension must be weighed against the distress to mother and infant resulting from the disruption in breast-feeding [88].

10.5.10.2   Renal Insufficiency

Nephrogenic systemic fibrosis (NSF) is a sclerosing disorder found in patients with impaired renal function after MRI examinations with gadolinium-based contrast agents (GBCA); symptoms usually develop up to 4 weeks after exposure. GBCA are renally eliminated, and so all patients with impaired renal function are at risk of retaining GBCA after exposure [89].

10.6   MRI in Diagnostics of TMJ

Magnetic resonance imaging (MRI) is claimed to be the method of choice for diagnosing TMJ involving soft tissue pathologies. MRI has been used to obtain information regarding especially articular disc position within the TMJ in patients. It provides a direct form of soft tissue visualization with excellent spatial and contrast resolution on sagittal and coronal MR images of the TMJ. The intra-articular disc composed of fibrous connective tissue and is located between the condyle and mandibular fossa. The disc divides the joint cavity into two comportments, called the lower and upper joint spaces, which are located below and above the disc, respectively. MRI can also provide essential information about position, morphology, and signal intensity characteristics of the TMJ structures (Figs. 10.24, 10.25, and 10.26).

10.6.1   MR Imaging of the TMJ Anatomy

In TMJ imaging although inflammation and fluid has low signal on T1W images, T2W images well depict both fluid and inflammatory changes with high signal intensity due to the increase in mobile protons resulting in a longer T2. The soft tissues of the bilaminar zone and lateral pterygoid attachments show moderate signal on T2W images but still lower than the T1W images. The signal returning from the yellow marrow is much lower than on T1W images due to the short T2 relaxation times of fat [90].

Fig. 10.24 Sagittal MR images showing anatomical landmarks. (1.) Lateral pterygoid muscle, (2.) articular eminence, (3.) maxillary sinus, (4.) temporal lobe of brain, (5.) external acoustic canal, (6.) mastoid air cells, (7.) sternocleidomastoid muscle, (8.) medial pterygoid muscle, (9.) masseter muscle
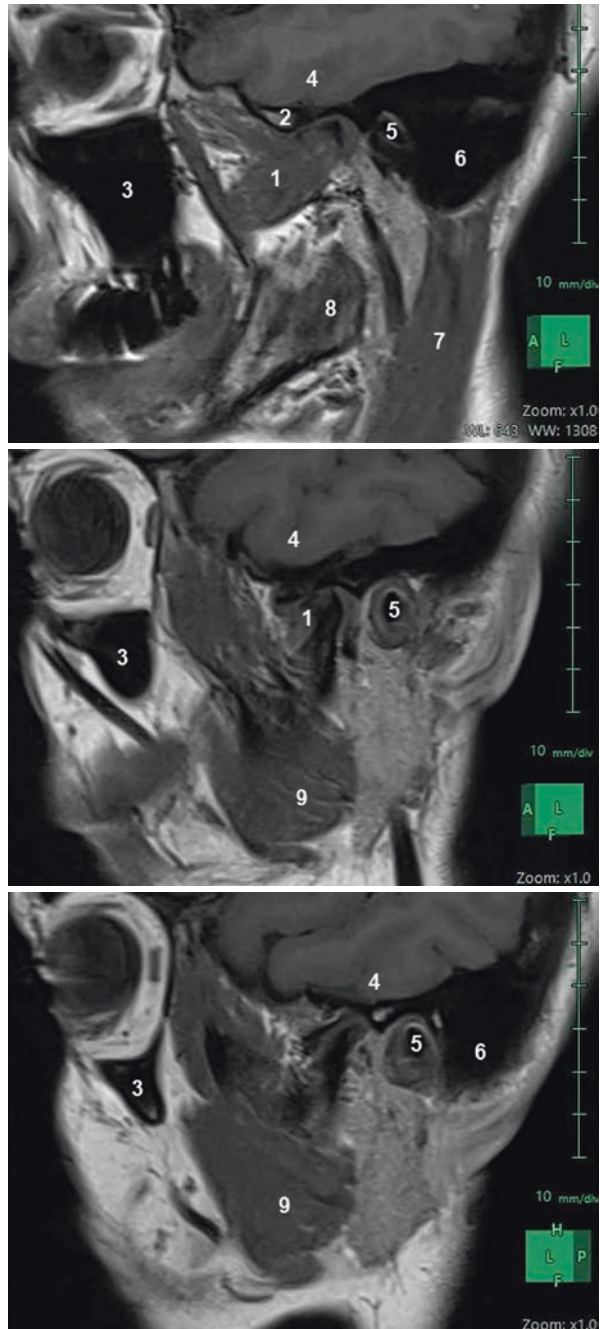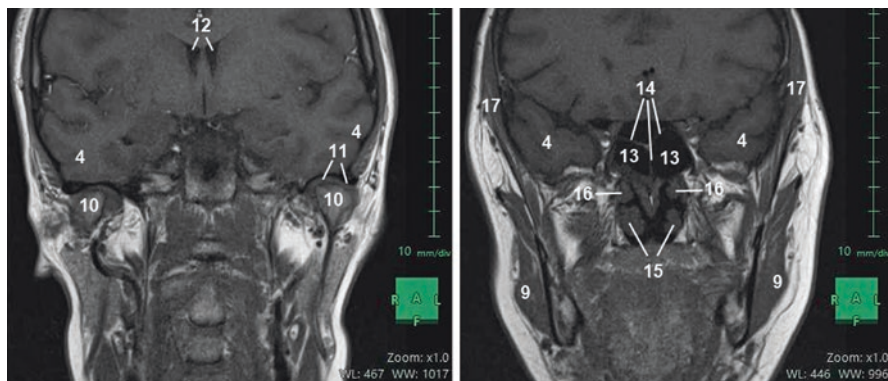
Fig. 10.25 Coronal MR images showing anatomical landmarks. 10. Condyle, (11.) disc, (12.) lateral ventricles, (13.) sphenoid sinus, (14.) sphenoid sinus septum, (15.) concha nasalis inferior, (16.) concha nasalis medius, (17.) temporal muscle
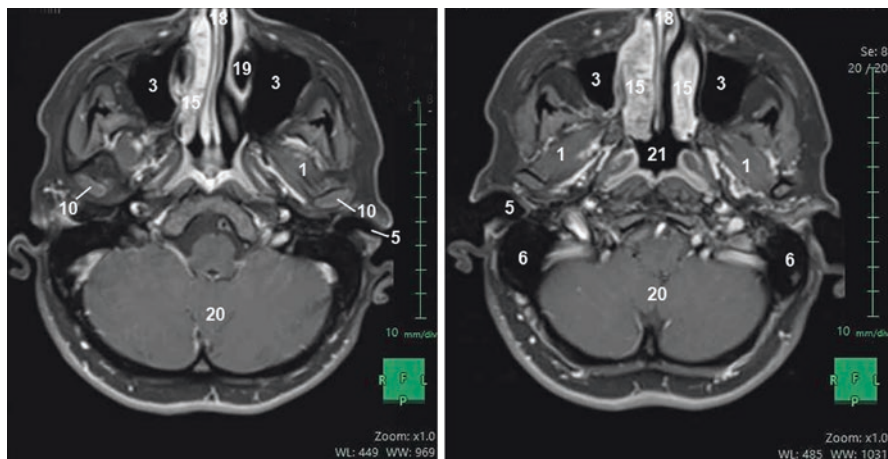
Fig. 10.26 Axial MR images showing anatomical landmarks. (18.) Nasal septum, (19.) nasolacrimal canal, (20.) cerebellum, (21.) nasopharynx

The yellow marrow within the condyle, zygomatic process, and articular eminence has a high signal due to its higher lipid content. The areas with intermediate signal are soft tissues in the bilaminar zone and lateral pterygoid attachments [90]. Temporomandibular joint (TMJ) disc presents low signal on T1W images [7, 90, 91]. Posterior disc attachment presents high signal relative to low signal in the posterior band of the fibrous disc [91].

In TMJ evaluation parasagittal and paracoronal T1W and PDW images in the closed mouth position best demonstrate the gross joint anatomy rather than T2W images [26, 92, 93]. TMJ disc still has low signal intensity unlike lateral pterygoid fat pat that shows high signal intensity (appears as bright) on PDW sequence [91]. While muscle exhibits intermediate signal intensity, fluid tends toward slightly higher or equal signal compared to muscle and cortical bone of the mandibular

condyle produce low signal intensity on PDW images [94]. Also posterior disc attachments present high signal intensity in contrast to the posterior band's lower signal [91, 95].

MR allows the imaging of the TMJ structures especially evaluating the disc position in both sagittal and coronal planes and the disc movement in open and closed mouth positions [96]. The articular disc is normally biconcave in shape and has three different parts including anterior (with intermediate thickness), intermediate (the thinnest part), and posterior band (the thickest part). Normally the posterior band of the articular disc lies at the superior or 12 o'clock position relative to the condyle when the jaw is in closed position. Centrally thinner intermediate zone of the articular disc lies between the condylar head and articular tubercle in open mouth position [91, 97–99], and medial part is thicker than the lateral part [7]. Usually low signal intensity of the avascular fibrous disc is well determined between the relatively high signals from the surrounding soft tissues lateral pterygoid muscle fat pat. Similarly cortex of the condyle has no signal; however, it is well demonstrated between the relatively high signal intensity of the cartilaginous and synovial tissue superiorly and bright signal of yellow marrow in the cancellous part of the condylar head inferiorly. In the coronal oblique plane, the disc has an arc-shaped configurations and is perfectly centered on the condyle and attached to the condylar poles [91] (Figs. 10.27 and 10.28).
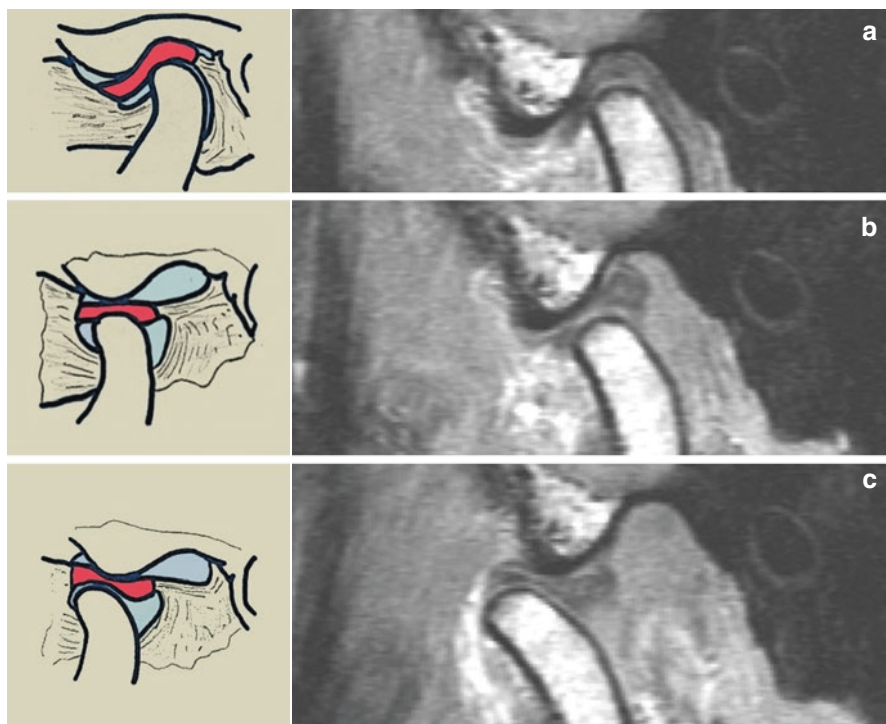

Fig. 10.27 MRI of a normal joint: (**a**) closed, (**b**) partially open, and (**c**) open mouth positions (derived from [97])
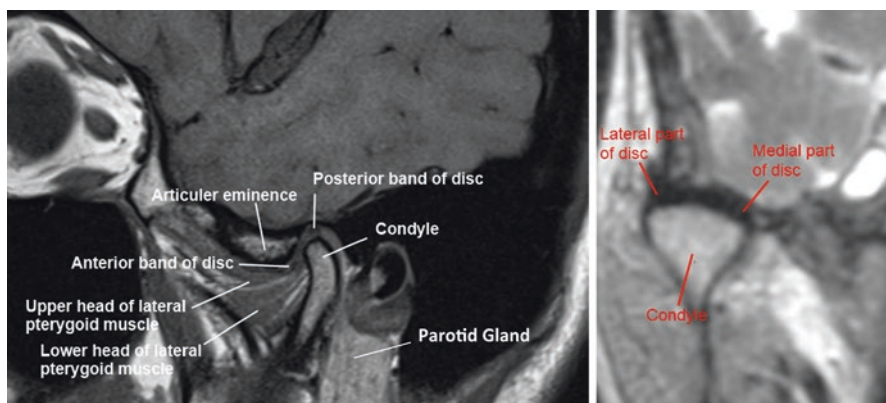
Fig. 10.28 Sagittal and coronal MR images showing the anatomical landmarks of TMJ

10.6.2 Disc Displacements

Temporomandibular disorders (TMD) are the most common nonodontogenic pain in the dentomaxillofacial region. Its prevalence is ranging between 16 and 68% and very variable depending on the study population, age, and gender [100]. However when evaluating the prevalence of joint pathology, the differences between objective diagnosis and subjective patient-reported pain are a challenging problem in terms of making a definitive diagnosis [97]. Disc displacements nearly affect up to one-third of asymptomatic volunteers in at least one TMJ [99, 101]. It is important to demonstrate the normal disc since some of the patients having TMD symptoms have normal disc [90]. In general, the most common breakdown in the masticatory system is the muscles, TMJs, and the dentition with developmental disorders. Among these groups, the disc displacements are the most encountered disorder type for TMJ.

Displacement or misalignment of the disc occurs when the disc is displaced from its normal position in relation to the head of the mandibular condyle in open and closed mouth position. Articular disc is most often displaced anteriorly. The type of the displacement may range partial or complete, uni- or multidirectional, and with or without reduction [7].

Partial anterior disc displacement (PADD): The disc is anteriorly misaligned in the lateral or medial part of the joint. The disc displaced in the medial or lateral slices but normally positioned in the other sagittal slices, which was not displaced laterally or medially in the coronal slices. If the disc is recaptured by the condyle and the disc condyle relationship appears normal when the jaw is opened, it was considered PADD [97, 98, 102] (Fig. 10.29).

Anterior disc displacement with reduction (ADDwR). In all sagittal sections, the posterior band of the disc is anterior position relative to the condylar head when the mouth is closed. While opening the mouth, the disc is recaptured by the condyle and returns to its normal position. In the maximum opening of the mouth disc–condyle relationship appears normally [97, 98, 102] (Fig. 10.30).

Fig. 10.29 T1-W image of partial anterior disc displacement (**a**) closed and (**b**) open mouth positions (derived from [97])
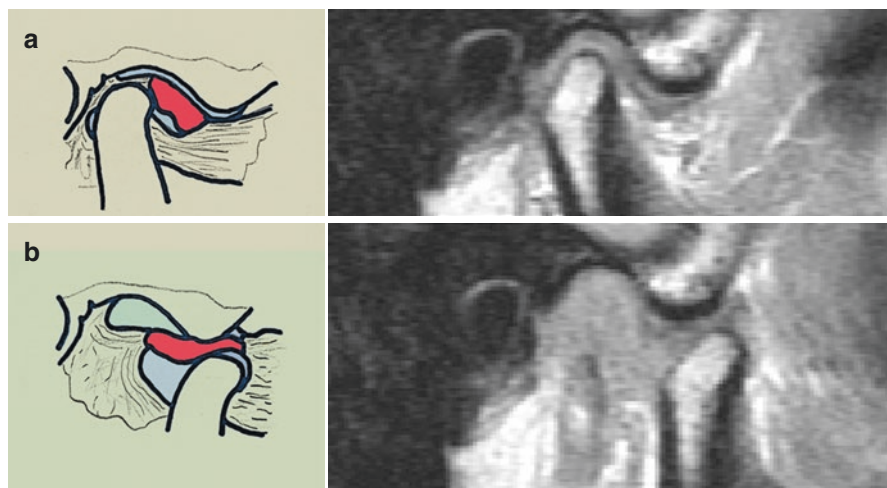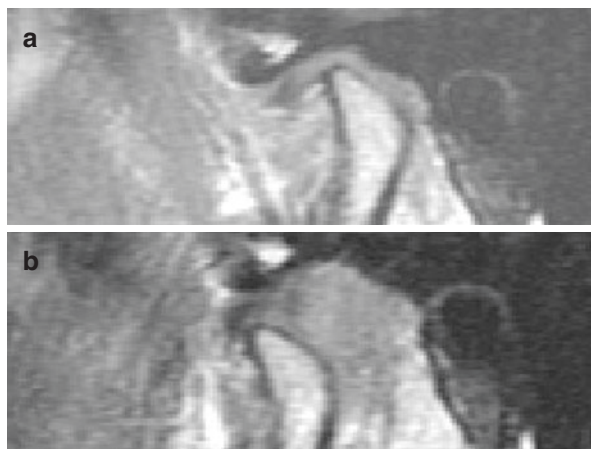

Fig. 10.30 MRI of ADDwR: (**a**) closed and (**b**) open mouths positions (derived from [97])

Anterior disc displacement without reduction (ADDwoR): In the closed mouth positions, the posterior band of the disc is anterior to the superior aspect of the condylar head in all sagittal sections and does not reduce during the mouth opening. When the jaw is opened, the disc is compressed anteriorly, regardless of whether its morphology is modified [97, 98, 102] (Fig. 10.31).

Sideways disc displacement (medial disc displacement/lateral disc displacement) (MDD/LDD without an anterior component): Sideways displacements of the disc are well depicted in the coronal plane. The disc crosses over one of the sagittal planes tangential to one of the condylar poles without an anterior component [91, 97, 98, 102] (Fig. 10.32).
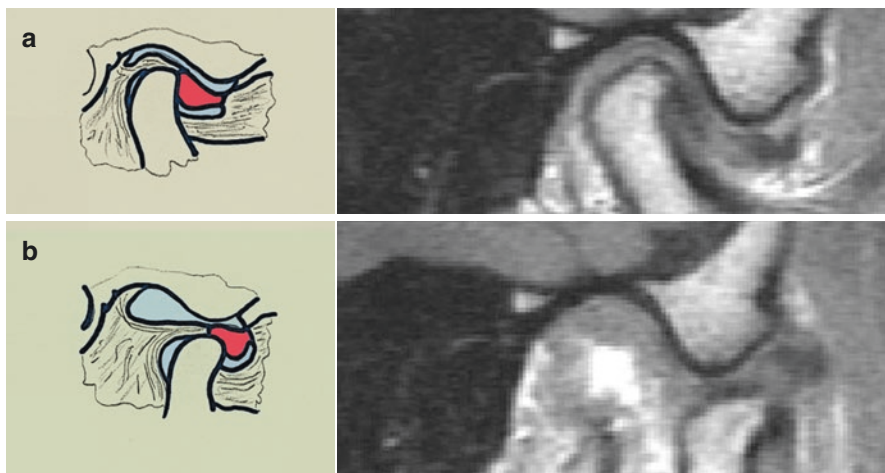
Fig. 10.31 MRI of ADDwoR: (**a**) closed and (**b**) open mouth positions (derived from [97])
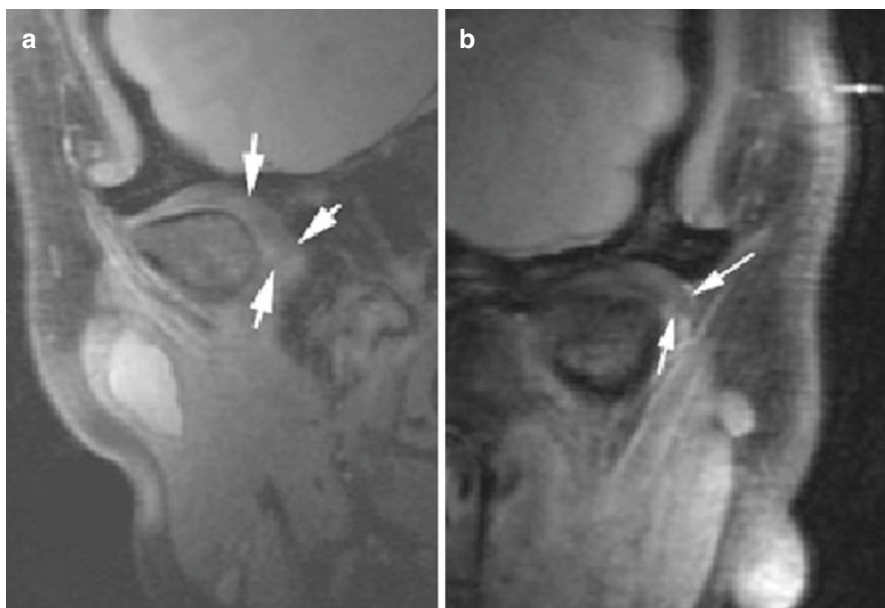

Fig. 10.32 MRI of (**a**) medial and (**b**) lateral disc displacement (derived from [97])

Stuck disc (STD) or disc adhesion: Although stuck disc is not a type disc displacement, they may occur together. A STD is defined as the disc remains in the same plane in relation to the mandibular fossa or articular tubercle during jaw movements [97, 98, 102] (Fig. 10.7).

Disc morphology may be classified into six categories: biconcave (a disc with clearly identifiable posterior and anterior bands and a tapered intermediate zone), biplanar (a disc with equal thickness in all three parts), biconvex (a humped disc), enlargement in the posterior band (a disc in which the posterior band is thicker and longer anteroposteriorly), Y shaped, and folded (irregular) [97]. Some researchers classified the disc morphology into the five categories according to disc shape: biconcave (both upper and lower surfaces are concave), biplanar (the disc is of even thickness), hemiconvex (upper surface is concave, while the lower is convex), biconvex (both upper and lower surfaces are convex), and folded (the disc is folded at the center) [102–104] (Fig. 10.33).

10.6.3 Bony Changes

Correlation between the MR imaging features and clinical symptoms of the TMD (such as pain) is still controversial. MR evidence of the joint effusion, condyle marrow suggesting edema, or osteonecrosis may be possible cause of the pain in TMJ.
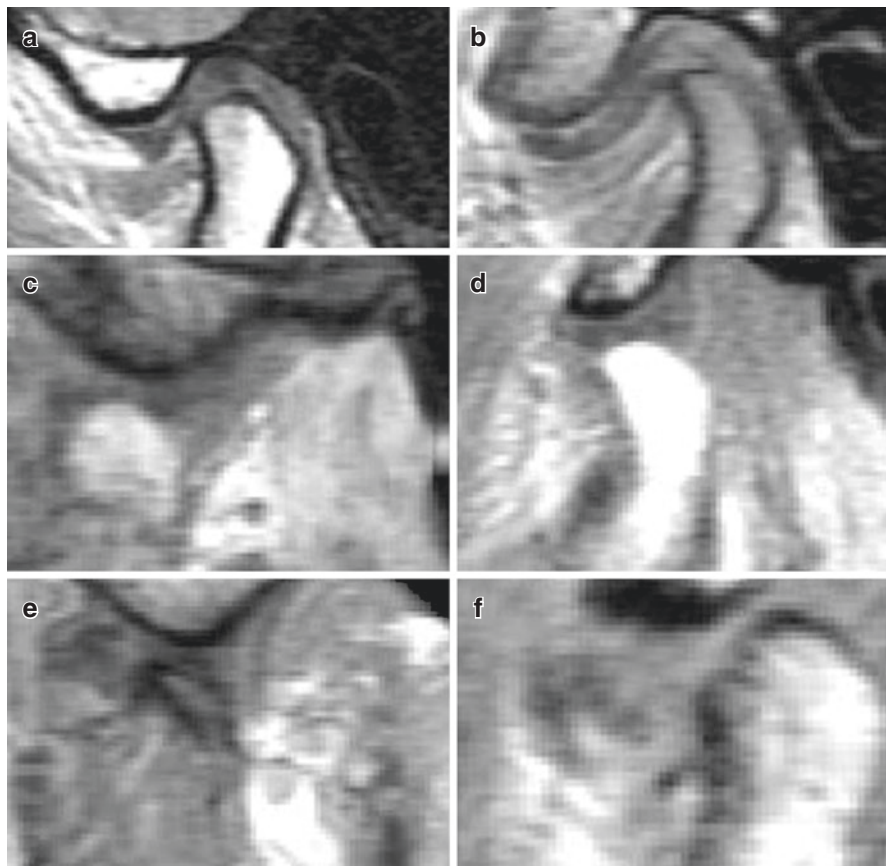

Fig. 10.33 MRI showing (**a**) biconcave disc, (**b**) biplane disc, (**c**) biconvex disc, (**d**) enlarged posterior band of the disc, (**e**) Y-shaped disc, and (**f**) folded disc (derived from [97])

For now, MRI is the only noninvasive imaging modality to evaluate the bone marrow in vivo. In MR images signal intensity is directly related to the relative content of fat, water, and cells in the marrow [30]. The normal bone marrow is hyperintense on T1W images and hypointense on T2W images. Reversal of these characteristics, decrease in signal intensity on T1W images, and bright signal on T2W images may be related with the medullary edema [92].

Bone marrow alterations may be categorized into three groups including normal bone marrow (homogeneous bright signal on proton density (PD) and homogeneous intermediate signal on T2-weighted images), marrow edema (decreased signal on PD and increased signal on T2-weighted images; edema pattern), and osteonecrosis (with decreased signal on PD and on T2-weighted images; sclerosis pattern or combination of edema pattern and sclerosis pattern; "combined" pattern) [105, 106]. Bone marrow edema may be a precursor condition for osteonecrotic development in temporomandibular disorder (TMD) patients [106–108] (Fig. 10.34).

Joint effusion which demonstrates the increased intra-articular fluid is classified into four groups including no fluid (no bright T2 signals from joint compartments), minimal fluid (dots or lines of bright T2 signals along articular surfaces), moderate fluid (more than the amount of bright T2 signals defined as minimal fluid and less than the amount defined as marked fluid), and marked fluid (equal to this amount of bright T2 signals or more) [105] (Figs. 10.5 and 10.6).
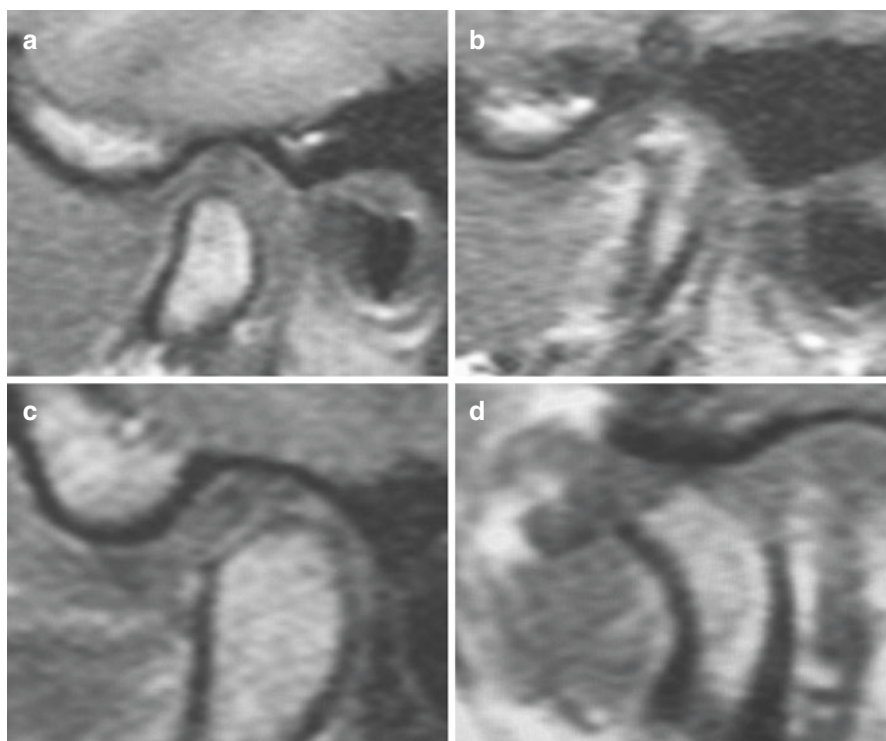

Fig. 10.34 Oblique sagittal T1-weighted MRI shows (**a**) normal condyle, (**b**) iso to high signal in condyle marrow consistent with bone marrow edema, (**c**) flattening of TMJ condyle, (**d**) mild osteoarthritis

There are many lesions both benign and malignant that can lead to bony destruction (see pathology) (Fig. 10.35). Apart from these lesions, several radiographic signs of the osteoarthritis are defined as osteophytes, subchondral sclerosis, generalized sclerosis, and cortical bone erosions [94]. Osteoarthritis appears as a focal
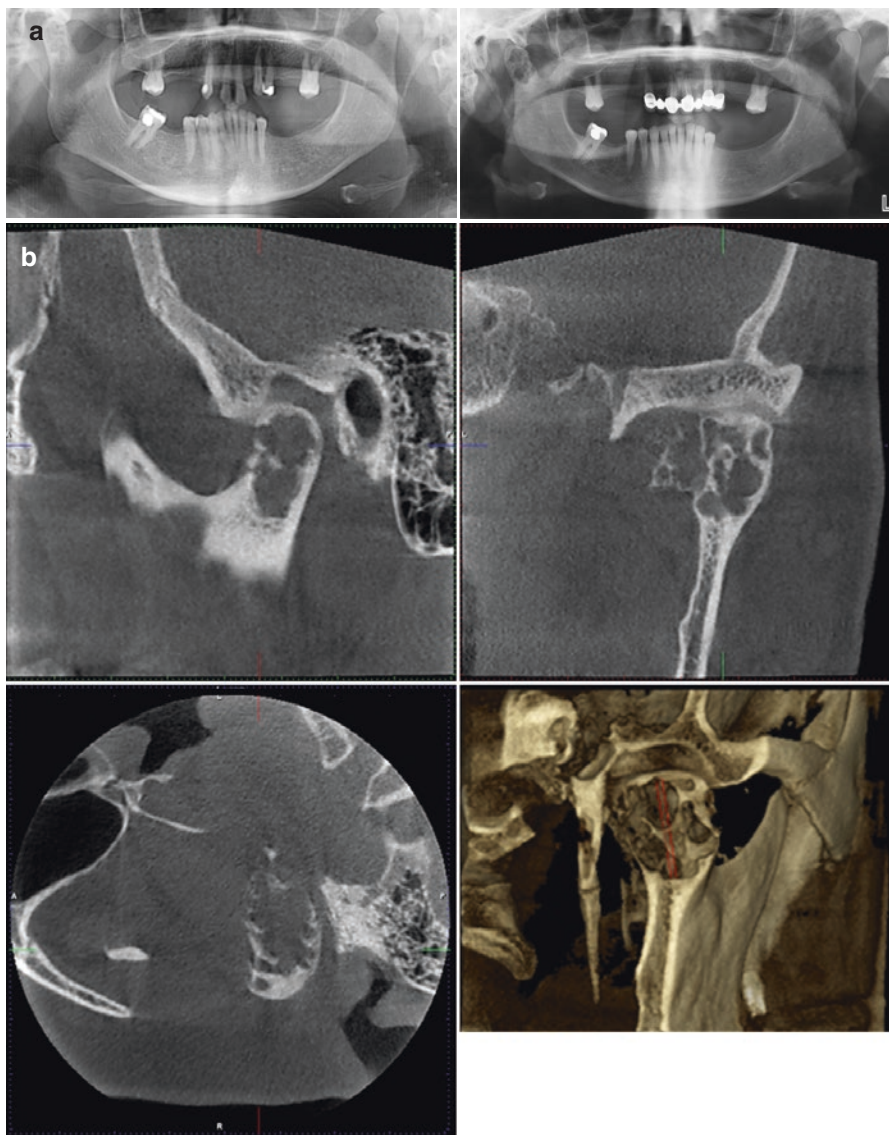

Fig. 10.35 A case of pigmented villonodular synovitis (PVNS) in a 62-year-old female patient, (**a**) panoramic radiographs in 2011 and 2017 with destruction of condyle, (**b**) CBCT images showing destruction with 3D reconstructions, (**c**) T1-W coronal image showing low signal, and (**d**) intermediate to high signal intensity in T2-W coronal image, (**e**) sagittal T1-W image enlarging mass extending around TMJ capsule, (**f**) DWI (b = 1000) showing the diffusion restriction area for the mass, (**g**) USG of the PVNS showing well vascularized hypo/isoechoic mass
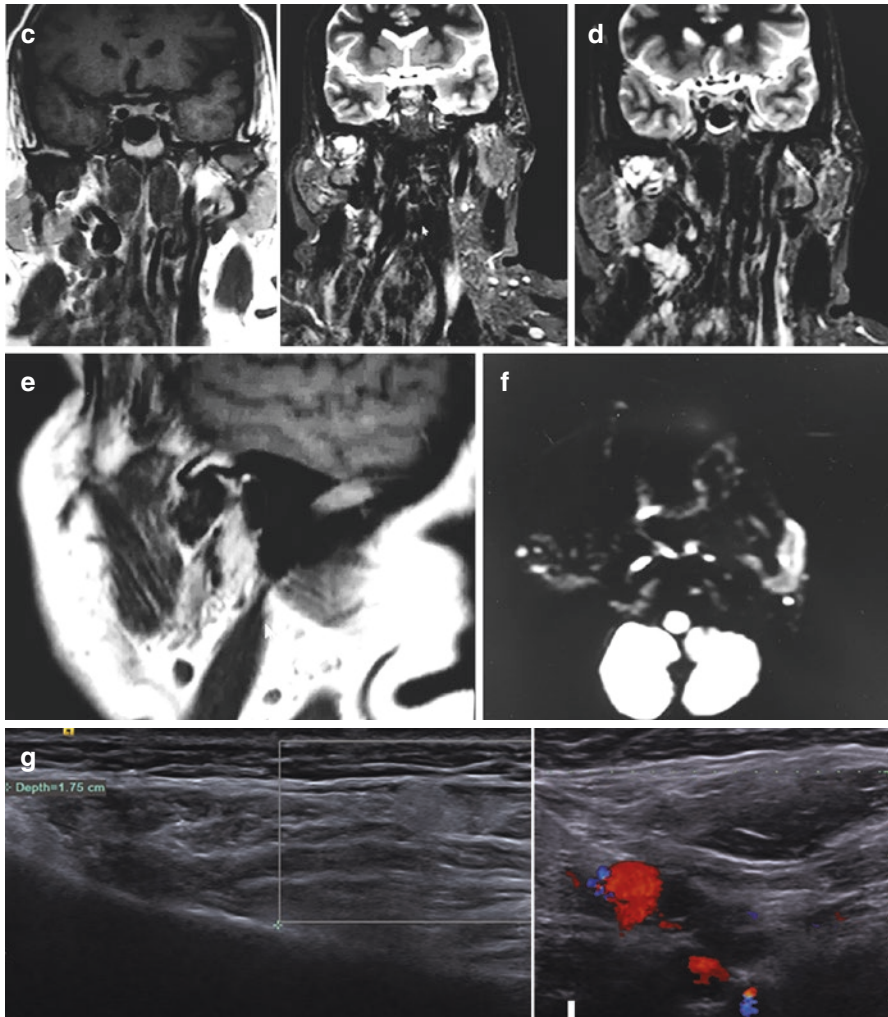
Fig. 10.35 (continued)

alteration (decrease) in signals on T1 and T2W images. Also focal increased signal on T2W images may show subchondral cyst [105]. Sclerosis represents low signal on both T1 and T2W images [109] (Fig. 10.36). More over, MRI is the modality of choice for confirming the diagnosis such as empty sella which shows same signal intensity with cerebrospinal fluid (Fig. 10.37).

Fig. 10.36 T2-W image showing high signal intensity of bone marrow and resorption of the condyle with perforation of the disc (arrows)
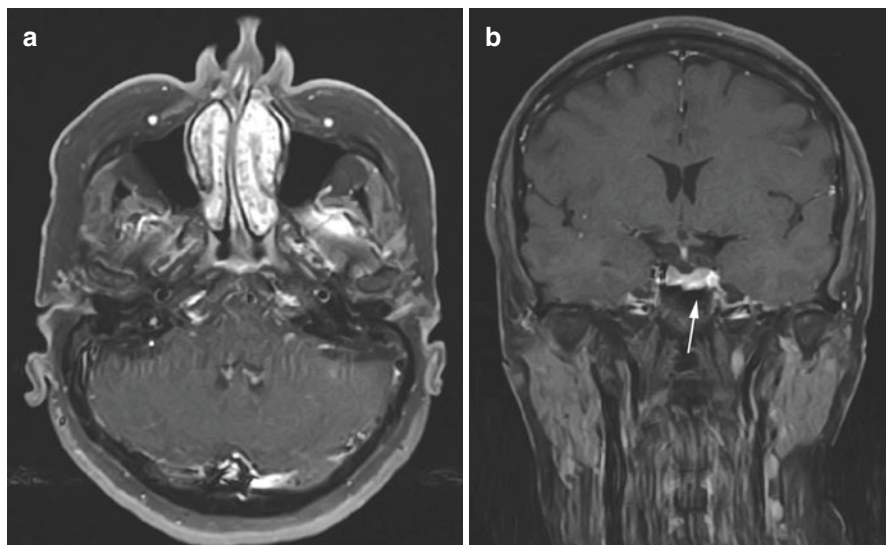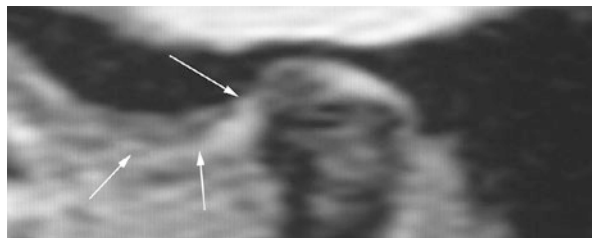

Fig. 10.37 (**a**) Axial, (**b**) coronal T1-W contrast-enhanced MR images showing a case of empty sella showing iso/high-intense signal intensity with CSF leak in the middle part of the sella (arrow)

References

1. Konez O. Manyetik rezonans görüntüleme temel bilgiler. İstanbul: Nobel Offset Matbaa; 1995.
2. Westbrook C, Roth CK, Talbot J, editors. MRI in practice. 4th ed. West Sussex: Wiley; 2011.
3. Weishaupt D, Köchli VD, Marincek B. How does MRI work? 2nd ed. Berlin: Springer; 2006.

 4. Bitar R, Leung G, Perng R, Tadros S, Moody AR, Sarrazin J, McGregor C, Christakis M, Symons S, Nelson A, Roberts TP. MR pulse sequences: what every radiologist wants to know but is afraid to ask. Radiographics. 2006;26(2):513–37.
 5. Gibby WA. Basic principles of magnetic resonance imaging. Neurosurg Clin N Am. 2005;16:1–64.
 6. Jacobson HG. Fundamentals of magnetic resonance imaging. Council on Scientific Affairs. JAMA. 1987;258:3417–23.
 7. White CS, Pharoah JM, editors. Oral radiology principles and interpretation. 7th ed. St.Louis: Mosby; 2014.
 8. Landini L, Positano L, Satanrelli MF, editors. Advanced image processing in magnetic reso-nance imaging. Boca Raton: Taylor and Francis Group; 2005.
 9. Brown MA, Semelka RC. MRI basıc principles and application. 3rd ed. New York: Wiley; 2003.
10. Diren BH. Manyetik Rezonans Görüntüleme temel bilgiler. Ankara: Mine Offset Matbaa; 1994.
11. Grover VP, Tognarelli JM, Crossey MM, Cox IJ, Taylor-Robinson SD, McPhail MJ. Magnetic resonance imaging: principles and techniques: lessons for clinicians. J Clin Exp Hepatol. 2015;5(3):246–55.
12. Collins CM. Electromagnetics in magnetic resonance imaging: physical principles, related applications, and ongoing developments. 1st ed. San Rafael: Morgan & Claypool Publishers; 2016.
13. Pooley RA. AAPM/RSNA physics tutorial for residents: fundamental physics of MR imaging. Radiographics. 2005;25(4):1087–99.
14. Runge MV, Nitz WR, Schmeets SH. The physics of clinical MR taught through images. 2nd ed. New York: Thieme; 2007.
15. Dietrich O, Raya JG, Reeder SB, Reiser MF, Schoenberg SO. Measurement of signal-to-noise ratios in MR images: influence of multichannel coils, parallel imaging, and reconstruction filters. J Magn Reson Imaging. 2007;26(2):375–85.
16. Scherzinger AL, Hendee WR. Basic principles of magnetic resonance imaging-an update. West J Med. 1985;143(6):782–92.
17. Jung BA, Weigel M. Spin echo magnetic resonance imaging. J Magn Reson Imaging. 2013;37(4):805–17.
18. Mangrum W, Christianson K, Duncan SM, Hoang P, Song AW, Merkle E. Duke review of MRI principles: case review series. 1st ed. Philadelphia: Elsevier; 2012.
19. Hennig J, Nauerth A, Friedburg H. RARE imaging: a fast imaging method for clinical MR. Magn Reson Med. 1986;3(6):823–33.
20. Calle D, Navarro T. Basic pulse sequences in magnetic resonance imaging. Methods Mol Biol. 2018;1718:21–37.
21. Delfaut EM, Beltran J, Johnson G, Rousseau J, Marchandise X, Cotten A. Fat suppression in MR imaging: techniques and pitfalls. Radiographics. 1999;19(2):373–82.
22. Brandão S, Seixas D, Ayres-Basto M, Castro S, Neto J, Martins C, Ferreira JC, Parada F. Comparing T1-weighted and T2-weighted three-point Dixon technique with conven-tional T1-weighted fat-saturation and short-tau inversion recovery (STIR) techniques for the study of the lumbar spine in a short-bore MRI machine. Clin Radiol. 2013;68(11):e617–23.
23. Ma J. Dixon techniques for water and fat imaging. J Magn Reson Imaging. 2008;28(3): 543–58.
24. Behr M, Held P, Leibrock A, Fellner C, Handel G. Diagnostic potential of pseudo-dynamic MRI (CINE mode) for evaluation of internal derangement of the TMJ. Eur J Radiol. 1996;23(3):212–5.
25. Lin WC, Lo CP, Chiang IC, Hsu CC, Hsu WL, Liu DW, Juan YH, Liu GC. The use of pseudo-dynamic magnetic resonance imaging for evaluating the relationship between tem-poromandibular joint anterior disc displacement and joint pain. Int J Oral Maxillofac Surg. 2012;41(12):1501–4.
26. Styles C, Whyte A. MRI in the assessment of internal derangement and pain within the tem-poromandibular joint: a pictorial essay. Br J Oral Maxillofac Surg. 2002;40(3):220–8.

27. Semelka RC, Kelekis NL, Thomasson D, Brown MA, Laub GA. HASTE MR imaging: description of technique and preliminary results in the abdomen. J Magn Reson Imaging. 1996;6(4):698–9.
28. Henzler T, Dietrich O, Krissak R, Wichmann T, Lanz T, Reiser MF, Schoenberg SO, Fink C. Half-Fourier-acquisition single-shot turbo spin-echo (HASTE) MRI of the lung at 3 tesla using parallel imaging with 32-receiver channel technology. J Magn Reson Imaging. 2009;30(3):541–6.
29. Morimoto Y, Tanaka T, Masumi SI, Tominaga K, Shibuya T, Kito S, et al. Significance of frequency-selective fat saturation T2-weighted MR images for the detection of bone marrow edema in the mandibular condyle. Cranio. 2004;22:115–23.
30. Orhan K, Delilbasi C, Paksoy C. Magnetic resonance imaging evaluation of mandibular condyle bone marrow and temporomandibular joint disc signal intensity in anaemia patients. Dentomaxillofac Radiol. 2009;38(5):247–54.
31. Tanaka T, Morimoto Y, Masumi S, Tominaga K, Ohba T. Utility of frequency-selective fat saturation T2-weighted MR images for the detection of joint effusion in the temporomandibular joint. Dentomaxillofac Radiol. 2002;31:305–12.
32. Barchetti F, Stagnitti A, Glorioso M, Al Ansari N, Barchetti G, Pranno N, et al. Static and dynamic MR imaging in the evaluation of temporomandibular disorders. Eur Rev Med Pharmacol Sci. 2014;18:2983–7.
33. Cassetta M, Barchetti F, Pranno N, Marini M. Comparing proton density and turbo spin echo T2 weighted static sequences with dynamic half-Fourier single-shot TSE pulse sequence at 3.0 T in diagnosis of temporomandibular joint disorders: a prospective study. Dentomaxillofac Radiol. 2014;43:1–7.
34. Wang EY, Mulholland TP, Pramanik BK, Nusbaum AO, Babb J, Pavone AG, et al. Dynamic sagittal half-Fourier acquired single-shot turbo spin-echo MR imaging of the temporomandibular joint: initial experience and comparison with sagittal oblique proton-attenuation images. Am J Neuroradiol. 2007;28:1126–32.
35. Conway WF, Hayes CW, Campbell RL. Dynamic magnetic resonance imaging of the temporomandibular joint using FLASH sequences. J Oral Maxillofac Surg. 1988;46:930–8.
36. Held P, Moritz M, Fellner C, Behr M, Gmeinwieser J. Magnetic resonance of the disk of the temporomandibular joint. MR imaging protocol. Clin Imaging. 1996;20:204–11.
37. Shimazaki Y, Saito K, Matsukawa S, Onizawa R, Kotake F, Nishio R, et al. Image quality using dynamic MR imaging of the temporomandibular joint with true-FISP sequence. Magn Reson Med Sci. 2007;6:15–20.
38. Schmid-Schwap M, Bristela M, Pittschieler E, Skolka A, Szomolanyi P, Weber M, et al. Biochemical analysis of the articular disc of the temporomandibular joint with magnetic resonance T2 mapping: a feasibility study. Clin Oral Investig. 2014;18:1865–71.
39. Widmann G, Henninger B, Kremser C, Jaschke W. MRI sequences in head & neck radiology—state of the art. Rofo. 2017;189(5):413–22.
40. Zhang S. Real-time magnetic resonance imaging [PhD thesis]. Goettingen: Georg-August-University; 2009.
41. Joseph AA. Real-time MRI of moving spins using undersampled radial FLASH [PhD thesis]. Bayerischen Julius-Maximilians-Universität Würzburg; 2013.
42. Wang X. Real-time MRI and model-based reconstruction techniques for parameter mapping of spin-lattice relaxation [PhD thesis]. Goettingen: Georg-August-University; 2016.
43. Roeloffs V, Voit D, Frahm J. Spoiling without additional gradients: radial FLASH MRI with randomized radiofrequency phases. Magn Reson Med. 2016;75:2094–9.
44. Uecker M, Thorsten H, Block KT, Frahm J. Image reconstruction by regularized nonlinear inversion—joint estimation of coil sensitivities and image content. Magn Reson Med. 2008;60:674–82.
45. Schaetz A, Voit D, Frahm J, Uecker M. Accelerated computing in magnetic resonance imaging – real-time imaging using non-linear inverse reconstruction. Comput Math Methods Med. 2017;2017:3527269.
46. Uecker M, Zhang S, Voit D, Merboldt KL, Frahm J. Real-time MRI: recent advances using radial FLASH. Imaging Med. 2012;4(4):1–22.

47. Niebergall A, Zhang S, Kunay E, Keydana G, Job M, Uecker M, et al. Real-time MRI of speaking at a resolution of 33 ms: Undersampled radial FLASH with 258 nonlinear inverse reconstruction. Magn Reson Med. 2013;69:477–85.

48. Iltis PW, Frahm J, Voit D, Joseph AA, Schoonderwaldt E, Altenmüller E. High speed real-time MRI of fast tongue movements in elite horn players. Quant Imaging Med Surg. 2015;5:374–81.

49. Olthoff A, Carstens PO, Zhang S, von Fintel E, Friede T, Lotz J, et al. Evaluation of dysphagia by novel real-time magnetic resonance imaging. Neurology. 2016;264(87):1–7.

50. Zhang S, Joseph AA, Gross L, Ghadimi M, Frahm J, Beham A. Diagnosis of gastroesophageal reflux disease using real-time magnetic resonance imaging. Sci Rep. 2015;5:12112. https://doi.org/10.1038/srep12112.

51. Kuriashkin IV, Losonsky JM. Contrast enhancement in magnetic resonance imaging using intravenous paramagnetic contrast media: a review. Vet Radiol Ultrasound. 2000;41(1):4–7.

52. Hodgson JR. The basic science of MRI. Orthop Trauma. 2011;25(2):119–30.

53. Ibrahim MA, Dublin AB. Magnetic resonance imaging (MRI), gadolinium. StatPearls [Internet]. Treasure Island: StatPearls Publishing; 2018.

54. Czeyda-Pommersheim F, Martin DR, Costello JR, Kalb B. Contrast agents for MR imaging. Magn Reson Imaging Clin N Am. 2017;25(4):705–11.

55. Currie S, Hoggard N, Craven IJ, Hadjivassiliou M, Wilkinson ID. Understanding MRI: basic MR physics for physicians. Postgrad Med J. 2013;89(1050):209–23.

56. Runge VM. Safety of approved MR contrast media for intravenous injection. J Magn Reson Imaging. 2000;12(2):205–13.

57. European Society of Magnetic Resonance in Medicine and Biology (ESMRMB) recommendation on adverse reactions to gadolinium based contrast agents (Gd-CA). 2008.

58. Dillman JR, Ellis JH, Cohan RH, Strouse PJ, Jan SC. Frequency and severity of acute allergic-like reactions to gadolinium-containing i.v. contrast media in children and adults. AJR Am J Roentgenol. 2007;189(6):1533–8.

59. Li A, Wong CS, Wong MK, Lee CM, Au Yeung MC. Acute adverse reactions to magnetic resonance contrast media—gadolinium chelates. Br J Radiol. 2006;79(941):368–71.

60. Thomsen HS, Webb JAW, editors. Contrast media. 2nd ed. Berlin: Springer; 2009. p. 123–8.

61. Hayat MA. Cancer imaging: instrumentation and applications. 1st ed. Amsterdam: Academic Press; 2007.

62. Cheong BY, Muthupillai R. Nephrogenic systemic fibrosis: a concise review for cardiologists. Tex Heart Inst J. 2010;37(5):508–15.

63. Marckmann P. An epidemic outbreak of nephrogenic systemic fibrosis in a Danish hospital. Eur J Radiol. 2008;66(2):187–90.

64. Cowper SE, Rabach M, Girardi M. Clinical and histological findings in nephrogenic systemic fibrosis. Eur J Radiol. 2008;66(2):191–9.

65. Thomsen HS, Marckmann P, Logager VB. Nephrogenic systemic fibrosis (NSF): a late adverse reaction to some of the gadolinium based contrast agents. Cancer Imaging. 2007;7:130–7.

66. Atkinson D, Hill DL, Stoyle PN, Summers PE, Clare S, Bowtell R, Keevil SF. Automatic compensation of motion artifacts in MRI. Magn Reson Med. 1999;41(1):163–70.

67. Pusey E, Yoon C, Anselmo ML, Lufkin RB. Aliasing artifacts in MR imaging. Comput Med Imaging Graph. 1988;12(4):219–24.

68. Hood MN, Ho VB, Smirniotopoulos JG, Szumowski J. Chemical shift: the artifact and clinical tool revisited. Radiographics. 1999;19(2):357–71.

69. Yanasak NE, Kelly MJ. MR imaging artifacts and parallel imaging techniques with calibration scanning: a new twist on old problems. Radiographics. 2014;34(2):532–48.

70. Stadler A, Schima W, Ba-Ssalamah A, Kettenbach J, Eisenhuber E. Artifacts in body MR imaging: their appearance and how to eliminate them. Eur Radiol. 2007;17(5):1242–55.

71. Arena L, Morehouse HT, Safir J. MR imaging artifacts that simulate disease: how to recognize and eliminate them. Radiographics. 1995;15(6):1373–94.

72. Taber KH, Herrick RC, Weathers SW, Kumar AJ, Schomer DF, Hayman LA. Pitfalls and artifacts encountered in clinical MR imaging of the spine. Radiographics. 1998;18(6):1499–521.

73. Klinke T, Daboul A, Maron J, Gredes T, Puls R, Jaghsi A, Biffar R. Artifacts in magnetic resonance imaging and computed tomography caused by dental materials. PLoS One. 2012;7(2):e31766.
74. Smeets R, Schöllchen M, Gauer T, Aarabi G, Assaf AT, Rendenbach C, Beck-Broichsitter B, Semmusch J, Sedlacik J, Heiland M, Fiehler J, Siemonsen S. Artefacts in multimodal imaging of titanium, zirconium and binary titanium-zirconium alloy dental implants: an in vitro study. Dentomaxillofac Radiol. 2017;46(2):20160267.
75. Poorsattar-Bejeh Mir A, Rahmati-Kamel M. Should the orthodontic brackets always be removed prior to magnetic resonance imaging (MRI)? J Oral Biol Craniofac Res. 2016;6(2):142–52.
76. Dalili Kajan Z, Khademi J, Alizadeh A, Babaei Hemmaty Y, Atrkar Roushan Z. A comparative study of metal artifacts from common metal orthodontic brackets in magnetic resonance imaging. Imaging Sci Dent. 2015;45(3):159–68.
77. Levine GN, Gomes AS, Arai AE, Bluemke DA, Flamm SD, Kanal E, Manning WJ, Martin ET, Smith JM, Wilke N, Shellock FS, American Heart Association Committee on Diagnostic and Interventional Cardiac Catheterization; American Heart Association Council on Clinical Cardiology; American Heart Association Council on Cardiovascular Radiology and Intervention. Safety of magnetic resonance imaging in patients with cardiovascular devices: an American Heart Association scientific statement from the Committee on Diagnostic and Interventional Cardiac Catheterization, Council on Clinical Cardiology, and the Council on Cardiovascular Radiology and Intervention: endorsed by the American College of Cardiology Foundation, the North American Society for Cardiac Imaging, and the Society for Cardiovascular Magnetic Resonance. Circulation. 2007;116(24):2878–91.
78. Dill T. Contraindications to magnetic resonance imaging: non-invasive imaging. Heart. 2008;94(7):943–8.
79. Campbell EA, Wilbert CD. Foreign body, imaging. SourceStat pearls [Internet]. Treasure Island: StatPearls Publishing; 2018.
80. Shellock FG, Crues JV. MRI: biologic effects, safety and patient management. 1st ed. Los Angeles: Biomedical Research Publishing Group; 2014.
81. Liebman CE, Messersmith RN, Levin DN, Lu CT. MR imaging of inferior vena caval filters: safety and artifacts. AJR Am J Roentgenol. 1988;150(5):1174–6.
82. Irnich W, Irnich B, Bartsch C, Stertmann WA, Gufler H, Weiler G. Do we need pacemakers resistant to magnetic resonance imaging? Europace. 2005;7(4):353–65.
83. Shellock FG. New metallic implant used for permanent contraception in women: evaluation of MR safety. AJR Am J Roentgenol. 2002;178(6):1513–6.
84. Öztürk E, Doruk C, Orhan KS, Çelik M, Polat B, Güldiken Y. A rare complication of Cochlear implantation after magnetic resonance imaging: reversion of the magnet. J Craniofac Surg. 2017;28(4):e372–4.
85. Tope WD, Shellock FG. Magnetic resonance imaging and permanent cosmetics (tattoos): survey of complications and adverse events. J Magn Reson Imaging. 2002;15(2):180–4.
86. Shellock FG, Crues JV. MR procedures: biologic effects, safety, and patient care. Radiology. 2004;232(3):635–52.
87. Dewey M, Schink T, Dewey CF. Claustrophobia during magnetic resonance imaging: cohort study in over 55,000 patients. J Magn Reson Imaging. 2007;26(5):1322–7.
88. Hylton NM. Suspension of breast-feeding following gadopentetate dimeglumine administration. Radiology. 2000;216(2):325–6.
89. Cowper SE. Nephrogenic systemic fibrosis: an overview. J Am Coll Radiol. 2008;5(1):23–8.
90. Harms SE, Wilk RM, Wolford LM, Chiles DG, Milam SB. The temporomandibular joint: magnetic resonance imaging using surface coils. Radiology. 1985;157(1):133–6.
91. Katzberg RW. Temporomandibular joint imaging. Radiology. 1989;170(2):297–307.
92. Alonso MBCC, Gamba TO, Lopes SLP, Cruz AD, Freitas DQ, Haiter-Neto F. Magnetic resonance imaging of the temporomandibular joint acquired using different parameters. J Morphol Sci. 2014;31(2):103–9.
93. Yang ZJ, Song DH, Dong LL, Li B, Tong DD, Li Q, Zhang FH. Magnetic resonance imaging of temporomandibular joint: morphometric study of asymptomatic volunteers. J Craniofac Surg. 2015;26(2):425–9.

94. Matthews NS. Dislocation of the Temporomandibular joint. 1st ed. New York: Springer; 2018.
95. Bag AK, Gaddikeri S, Singhal A, Hardin S, Tran BD, Medina JA, Curé JK. Imaging of the temporomandibular joint: an update. World J Radiol. 2014;6(8):567–82.
96. Brooks SL, Brand JW, Gibbs SJ, Hollender L, Lurie AG, Omnell KA, Westesson PL, White SC. Imaging of the temporomandibular joint: a position paper of the American Academy of Oral and Maxillofacial Radiology. Oral Surg Oral Med Oral Pathol Oral Radiol Endod. 1997;83(5):609–18.
97. Arslan A, Orhan K, Paksoy SC, Ucok O, Ozbek M, Dural S, Kanli A. MRI evaluation of the classification, frequency and disk morphology of temporomandibular joint disk displacement: a multicenter retrospective study in a Turkish population. Oral Radiol. 2009;25:14–21.
98. Foucart JM, Carpentier P, Pajoni D, Marguelles-Bonnet R, Pharaboz C. MR of 732 TMJs: anterior, rotational, partial and sideways disc displacements. Eur J Radiol. 1998;28(1):86–94.
99. Tasaki MM, Westesson PL, Isberg AM, Ren YF, Tallents RH. Classification and prevalence of temporomandibular joint disk displacement in patients and symptom-free volunteers. Am J Orthod Dentofac Orthop. 1996;109(3):249–62.
100. Sena MF, Mesquita KS, Santos FR, Silva FW, Serrano KV. Prevalence of temporomandibular dysfunction in children and adolescents. Rev Paul Pediatr. 2013;31(4):538–45.
101. Katzberg RW, Westesson PL, Tallents RH, Drake CM. Anatomic disorders of the temporomandibular joint disc in asymptomatic subjects. J Oral Maxillofac Surg. 1996;54(2):147–53. discussion 153–5.
102. Orhan K, Nishiyama H, Tadashi S, Murakami S, Furukawa S. Comparison of altered signal intensity, position, and morphology of the TMJ disc in MR images corrected for variations in surface coil sensitivity. Oral Surg Oral Med Oral Pathol Oral Radiol Endod. 2006;101(4):515–22.
103. Murakami S, Takahashi A, Nishiyama H, Fujishita M, Fuchihata H. Magnetic resonance evaluation of the temporomandibular joint disc position and configuration. Dentomaxillofac Radiol. 1993;22(4):205–7.
104. Taşkaya-Yilmaz N, Oğütcen-Toller M. Magnetic resonance imaging evaluation of temporomandibular joint disc deformities in relation to type of disc displacement. J Oral Maxillofac Surg. 2001;59(8):860–6.
105. Larheim TA, Katzberg RW, Westesson PL, Tallents RH, Moss ME. MR evidence of temporomandibular joint fluid and condyle marrow alterations: occurrence in asymptomatic volunteers and symptomatic patients. Int J Oral Maxillofac Surg. 2001;30(2):113–7.
106. Larheim TA, Westesson PL, Hicks DG, Eriksson L, Brown DA. Osteonecrosis of the temporomandibular joint: correlation of magnetic resonance imaging and histology. J Oral Maxillofac Surg. 1999;57(8):888–99.
107. Sano T, Westesson PL, Larheim TA, Rubin SJ, Tallents RH. Osteoarthritis and abnormal bone marrow of the mandibular condyle. Oral Surg Oral Med Oral Pathol Oral Radiol Endod. 1999;87(2):243–52.
108. Sano T. Recent developments in understanding temporomandibular joint disorders. Part 1: bone marrow abnormalities of the mandibular condyle. Dentomaxillofac Radiol. 2000;29(1):7–10.
109. Lieberman JM, Gardner CL, Motta AO, Schwartz RD. Prevalence of bone marrow signal abnormalities observed in the temporo-mandibular joint using magnetic resonance imaging. J Oral Maxillofac Surg. 1996;54:434–9.